2014

THE DIFFERENCES BETWEEN IRON AND IRON-SUBSTITUTED MANGANESE SUPEROXIDE DISMUTASE WITH RESPECT TO HYDROGEN PEROXIDE TREATMENT

Jianing Wang
University of Kentucky, yearalit@hotmail.com

STUDENT AGREEMENT:

I represent that my thesis or dissertation and abstract are my original work. Proper attribution has been given to all outside sources. I understand that I am solely responsible for obtaining any needed copyright permissions. I have obtained needed written permission statement(s) from the owner(s) of each third-party copyrighted matter to be included in my work, allowing electronic distribution (if such use is not permitted by the fair use doctrine) which will be submitted to UKnowledge as Additional File.

I hereby grant to The University of Kentucky and its agents the irrevocable, non-exclusive, and royalty-free license to archive and make accessible my work in whole or in part in all forms of media, now or hereafter known. I agree that the document mentioned above may be made available immediately for worldwide access unless an embargo applies.

I retain all other ownership rights to the copyright of my work. I also retain the right to use in future works (such as articles or books) all or part of my work. I understand that I am free to register the copyright to my work.

REVIEW, APPROVAL AND ACCEPTANCE

The document mentioned above has been reviewed and accepted by the student's advisor, on behalf of the advisory committee, and by the Director of Graduate Studies (DGS), on behalf of the program; we verify that this is the final, approved version of the student's thesis including all changes required by the advisory committee. The undersigned agree to abide by the statements above.

Jianing Wang, Student

Dr. Jianing Wang, Major Professor

Dr. Dongsheng Yang, Director of Graduate Studies

THE DIFFERENCES BETWEEN IRON AND IRON-SUBSTITUTED MANGANESE SUPEROXIDE DISMUTASE WITH RESPECT TO HYDROGEN PEROXIDE TREATMENT

THESIS

A thesis submitted in partial fulfillment of the
requirements for the degree of Master of Chemistry in the
College of Arts and Sciences
at the University of Kentucky

By
Jianing Wang

Lexington, Kentucky

Director Dr. Anne-Frances Miller, Professor of Chemistry

Lexington, Kentucky

2014

ABSTRACT OF THESIS

THE DIFFERENCES BETWEEN IRON AND IRON-SUBSTITUTED MANGANESE SUPEROXIDE DISMUTASE WITH RESPECT TO HYDROGEN PEROXIDE TREATMENT

Iron-substituted manganese superoxide dismutase (Fe(Mn)SOD) was produced using an *in vivo* preparation method. It's an inactive enzyme in catalyzing superoxide radical dismutation owing to the mis-incorporation of Fe in the active site evolved to use Mn. To investigate the possible toxicity of human Fe(Mn)SOD proposed by Yamakura[1], we studied the properties of Fe(Mn)SOD upon H_2O_2 treatment and compared to that of FeSOD. It's found that the responses to H_2O_2 treatment were different, including the changes of optical spectra, variations of active site coordination and secondary structures. Fe^{3+} reduction was not observed in Fe(Mn)SOD even H_2O_2 is believed to oxidize proteins via highly reactive intermediates including Fe and formed via Fe^{2+}, which is true in FeSOD. What's more, the activities of Fe(Mn)SOD and FeSOD were totally different in the ABTS assay or Amplex Red assay. These results indicated that the mechanism of peroxidase reaction of Fe(Mn)SOD is not identical to that of FeSOD.

KEYWORDS: Iron-substituted manganese superoxide dismutase, Hydrogen peroxide treatment, Tryptophan modification, secondary structure loss, Alternate substrate oxidation

Jianing Wang
Author's Signature

May 8, 2014
Date

THE DIFFERENCES BETWEEN IRON AND IRON-SUBSTITUTED MANGANESE SUPEROXIDE DISMUTASE WITH RESPECT TO HYDROGEN PEROXIDE TREATMENT

By

Jianing Wang

Anne-Frances Miller, PhD
Director of Thesis

Dongsheng Yang, PhD
Director of Graduate Studies

May 8, 2014
Date

Table of Contents

LIST OF TABLES

LIST OF FIGURES

Chapter 1 Introduction of iron-substituted manganese superoxide dismutase (Fe(Mn)SOD)

Oxygen plays an essential role in the cellular metabolism as the terminal electron acceptor for respiration, and a participant in other reactions[2-5]. Many compounds need to be oxidized as part of their metabolism. Respiratory electron transfer and coupled ATP production is the major source of energy for animals. The correct product of respiratory O_2 reduction is 2 H_2O. However, biproducts of reduction of oxygen are partially reduced species such as H_2O_2 and $O_2^{\bullet-}$ (hydrogen peroxide an superoxide), which are very reactive and can be harmful to cells[6-10]. Many diseases and the aging of humans are found to be related to the abundance and activities of reactive oxygen species (ROS)[11-13]. Therefore it is not surprising that all known aerobic organisms possess superoxide dismutases (SOD), which catalyze the disproportionation of superoxide radical ($O_2^{\bullet-}$), an ROS that gives rise to several of the other ROS.

The overall dismutation reaction of superoxide is shown in equation (1) and the mechanism of SOD has been studied for several decades[14-19]. There are three types of SOD based on the protein fold and the identity of the metal ion involved in catalysis. One type of SOD employs nickel, another uses binuclear copper/zinc, and the third utilizes either iron or manganese in the active site. Although the third family includes SODs that harbor either iron (FeSOD) or manganese (MnSOD), the proteins are homologous based on their similar amino acid sequences, structures and active site geometries[20]. The ribbon structure and active site of FeSOD are shown in Figure 1-1 and 1-2, repsectively. Many organisms contain multiple different types of SOD. For example, *Escherichia coli* has MnSOD, FeSOD and Cu, Zn-SOD[21]. The published crystal structures of FeSOD and MnSOD from *E. coli* demonstrate that the active sites are almost superimposable[22], as indicated in Figure 1-3, and their amino acid sequences are 44% identical. Thus, although the two proteins employ different metal ions

to catalyze superoxide dismutation, the proteins are very similar. In both cases the reaction occurs via alternate oxidation and reduction of superoxide as the active metal ion cycles from the 3+ state to the 2+ state and back. The general catalytic mechanism of FeSOD and MnSOD is shown in equation (2) and (3) as follows:

$$O_2^{\bullet -} + H_2O_2 \rightarrow OH^- + OH^{\bullet} + O_2 \quad (1)$$

$$O_2^{\bullet -} + H^+ + SOD(M^{3+} - OH^-) \rightarrow O_2 + SOD(M^{2+} - OH_2) \quad (2)$$

$$O_2^{\bullet -} + H^+ + SOD(M^{2+} - OH_2) \rightarrow H_2O_2 + SOD(M^{3+} - OH^-) \quad (3)$$

Given the similarities between FeSOD and MnSOD, it is not surprising that the MnSOD protein can bind Fe, to produce iron-substituted MnSOD ('Fe(Mn)SOD hereafter). The active site of Fe(Mn)SOD is superimposable with that of FeSOD[22] but Fe(Mn)SOD is inactive in the standard assay. This has been explained on the basis of redox tuning. Because high spin $Mn^{3+/2+}$ has a considerably higher reduction midpoint than does $Fe^{3+/2+}$ the MnSOD protein depressed the midpoint potential of its bound metal ion much more than does the FeSOD protein. Thus Fe(Mn)SOD has a much lower reduction midpoint potential than FeSOD[23,24]. Fe^{3+}(Mn)SOD also has a higher affinity for small anions than does Fe^{3+}SOD, so that OH^- binds as a sixth ligand at pH 6.7[23] as opposed to pH 9 for FeSOD[25]. Therefore the Fe center of Fe(Mn)SOD is seen to be distorted from trigonal bipyramidal to tetragonal coordination owing to the bound hydroxide as a sixth ligand[22].

MnSOD is the major active antioxidant enzyme in human mitochondria [26,27], and FeSOD is absent. The activity of MnSOD is very important for mitochondrial function and integrity. Many cancer cells show abnormal MnSOD protein expression or catalytic activity. St. Clair and coworkers[28] proposed that imperfect MnSOD synthesis may occur due to gene mutation, short and immature mRNA transcripts or inappropriate metal incorporation, which could be the Fe-substituted form.

Studies[29-31] have showed that when mitochondrial iron homeostasis is disrupted or when cells are short for manganese, iron accumulates and binds to MnSOD[29-31]. Incorporation of the “wrong" metal ion into the SOD active site results in inactive enzyme and the exacerbation of oxidative stress. Unfortunately, the metal uptake process only possesses modest selectivity both *in vivo* and *in vitro*[32-36]. Competition between iron and manganese for active site binding occurs based on the availability of these metal ions in the matrix. Mn access to apo-MnSOD is important for enzyme functional maturation, but steps governing it are still not clear. Whittaker’s group[37-41] have spent lots of effort studying the mechanism of metal uptake by MnSOD both *in vivo* and *in vitro*. They found that the metallation process depended on temperature, suggesting a conformational gate. Therefore they proposed that SOD metallation required either subunit dissociation or domain separation[42]. This provided a new insight into the metallation mechanism of the SOD apoprotein, which is likely to be conserved over this family of enzymes.

Recently, Yamakura [1] proposed that Fe(Mn)SOD possesses a radical-generating activity against 2,2’-azinobis-(3-ethylbenzthiazoline-6-sulfonate) (ABTS) in the presence of H_2O_2. The mechanism of radical formation by Fe(Mn)SOD and H_2O_2 is unknown and complicated since FeSOD and MnSOD have different responses to peroxide treatment. FeSOD is reduced and inactivated by H_2O_2 [43-45], whereas MnSOD is generally resistant[46,47]. In the current study, we find that Fe(Mn)SOD is able to react with H_2O_2 in the absence of ABTS. The results indicated that the mechanism of this reaction is not identical to that of FeSOD. The initiation of the reaction might not be result from Fe^{3+} reduction since no Fe^{3+} signal is lost based on both optical and EPR spectra. Fluorescence spectroscopy and circular dichroism indicate that tryptophan residues are modified and local secondary structure of the enzyme is lost, possibly because of the radicals formed.

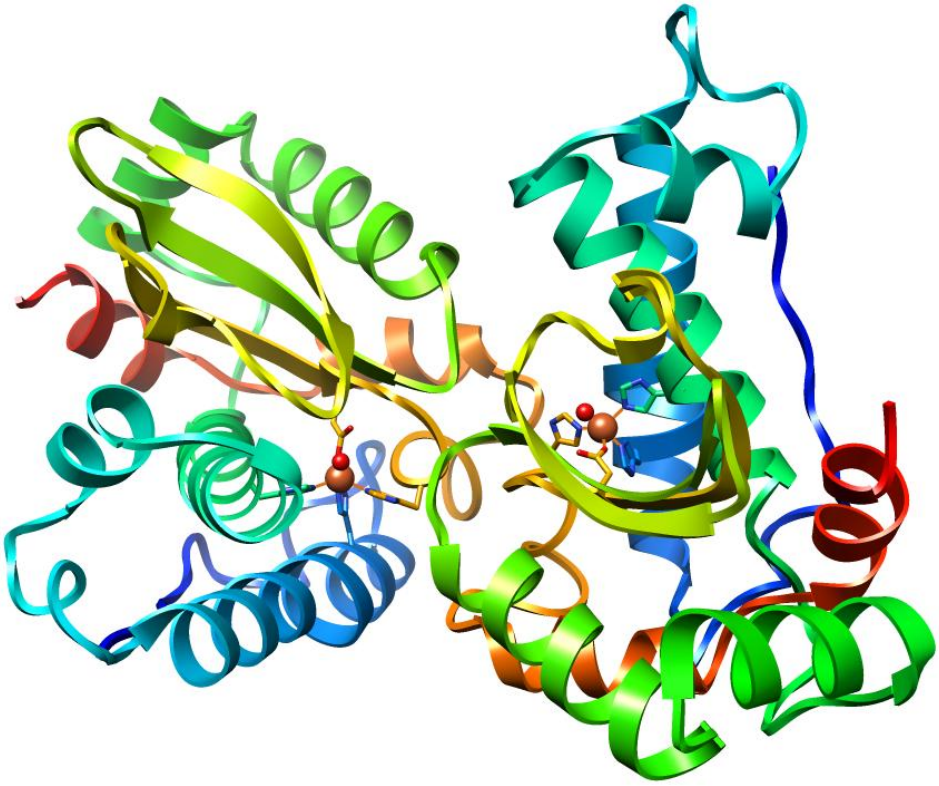

Figure 1-1 Ribbon structure of E. *coli* Fe^{3+}SOD dimer.
Fe^{3+} is shown as a large orange sphere and the heavy atoms of the ligands are from C_α out in stick format. Based on the coordinates of Fe^{3+}SOD published by Lah *et al.*, 1ISB,[48] and produced by Miller, A. F. using CHIMERA.

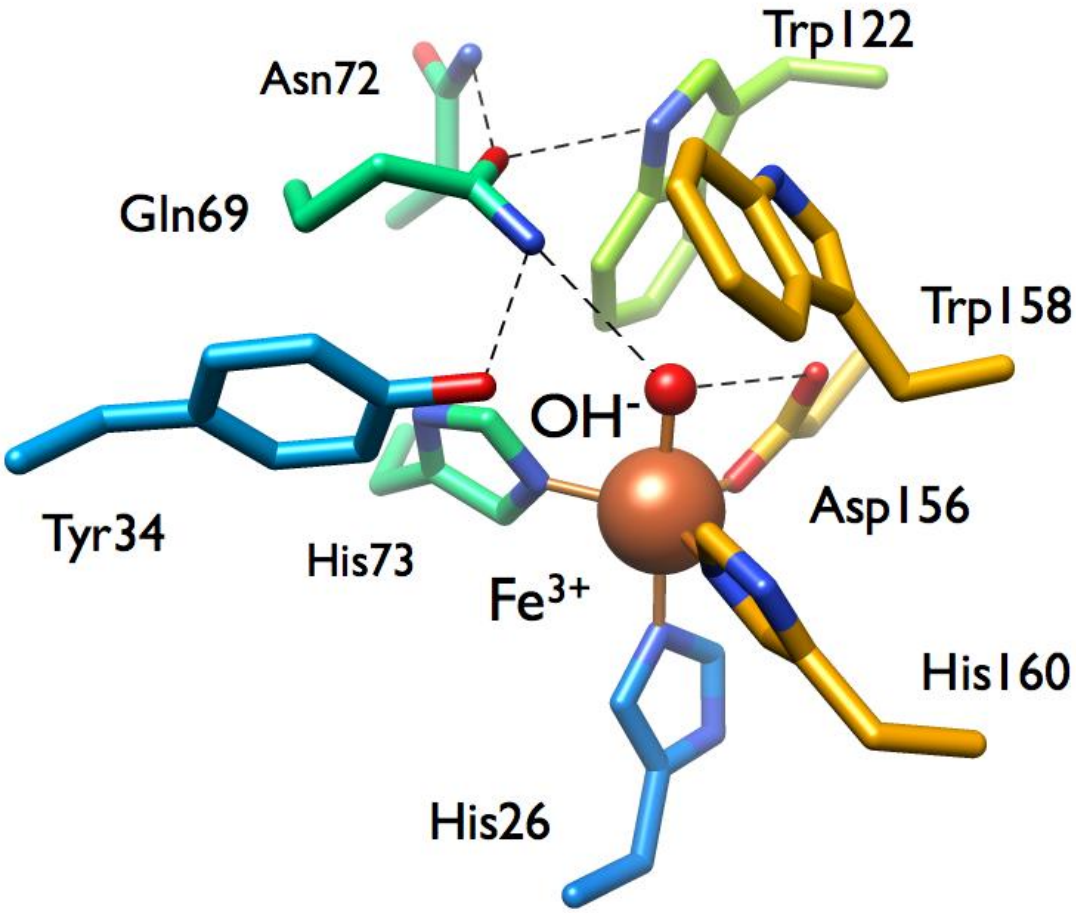

Figure 1-2 The active site in FeSOD.
The active site including selected second sphere residues in FeSOD with commonly-reported hydrogen bonds. H atoms and backbone atoms are omitted for clarity. Color-coded residues retain the same coloring as in Figure 1-1. Based on the coordinates of Fe^{3+}SOD published by Lah *et al.*, 1ISB,[48] and produced by Miller, A. F. using CHIMERA.

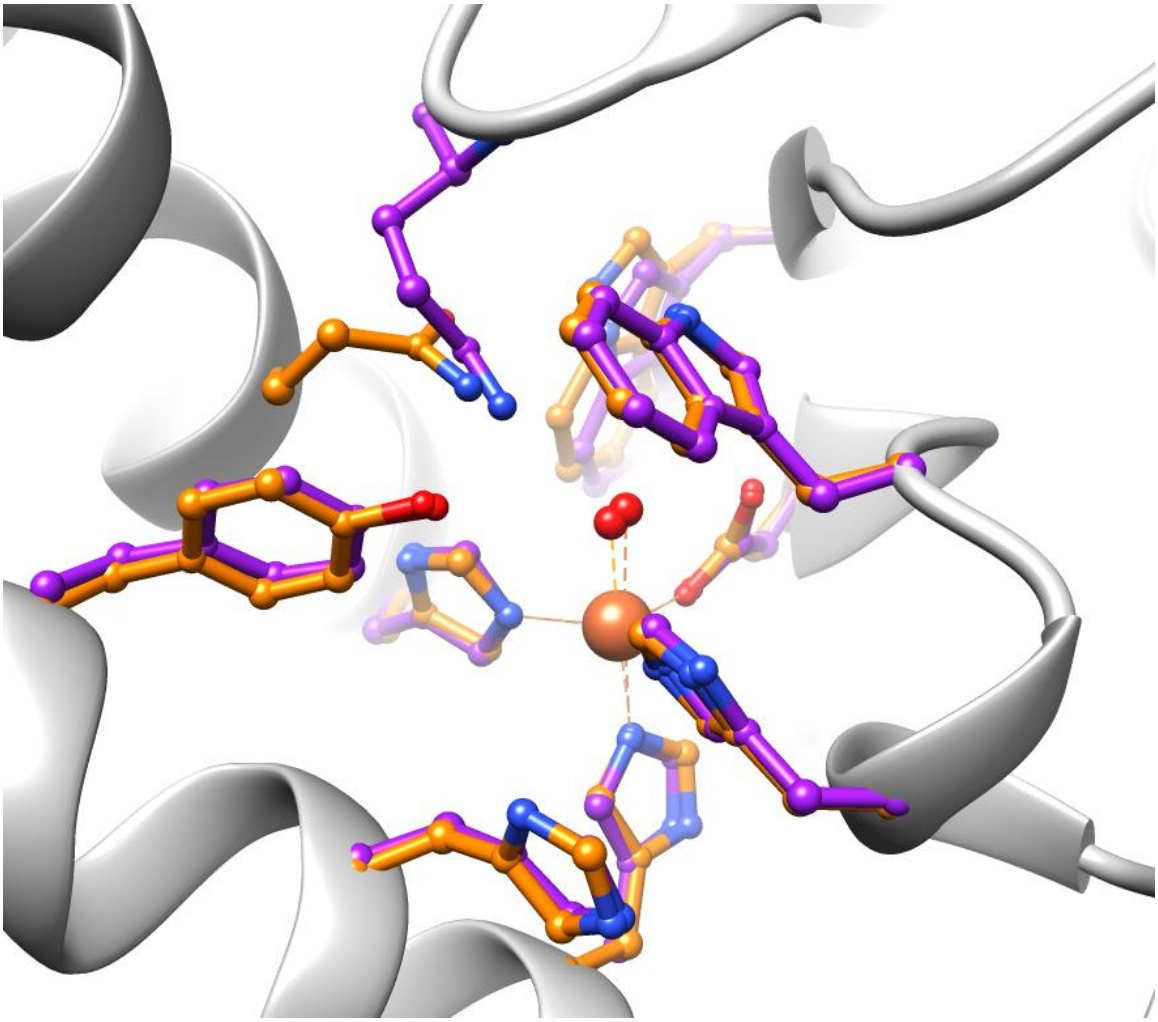

Figure 1-3 Overlay of the active sites of Fe^{3+}(Mn)SOD and Fe^{3+}SOD.
Overlay of the active sites of Fe^{3+}(Mn)SOD (magenta Cs) and Fe^{3+}SOD (orange Cs) based on the A-chain coordinates of Edwards et al. (1MMM)[22] and the A chain coordinates of Lah et al. (1ISB) [48]. Produced by Miller, A. F. using CHIMERA.

Chapter 2 Fe(Mn)SOD protein *in vivo* overexpression, purification and characterization

2.1 Introduction

Many studies of Fe(Mn)SOD have been published. In most of them Fe(Mn)SOD proteins were obtained from MnSOD after denaturing it, removing Mn, and then refolding in the presence of Fe [36,42,49,50]. Unfortunately, it is very hard to prevent non-specific binding of Fe to the protein, when attempting to provide Fe for the active site. Fe bound outside the active site (non-active site Fe, NAS-Fe) contributes to the optical and the EPR spectra, and have the possibility of compete with active site Fe in ligand binding[23]. Besides, the denaturing and refolding process are also time and energy consuming, and introduce the risk of unexpected modifications to the protein.

To avoid this, we sought to overexpress MnSOD protein in *E. coli* and obtain Fe(Mn)SOD *in vivo* by manipulating the Fe and Mn supplied to the culture. This could be plausible since competition between Fe and Mn for active site binding is known to occur *in vivo*, generating MnSOD protein containing Fe or Fe and Mn, as well as MnSOD[32,33]. Studies also indicated that some conditions could be chosen to favor Fe binding, such as a high concentration of Fe (II), and anaerobic growth conditions. Benov has pointed out that iron-enriched medium imposed on *E. coli* and inhibited SOD formation[51], so we used a lower concentration of Fe (II) that has been found to be non-inhibitory in other circumstances.

This chapter describes our method of producing Fe(Mn)SOD *in vivo*, and the properties of the material that results.

2.2 Materials and Methods

The wild type MnSOD gene from *E. coli* on the pET21a derivative pAK0 was transformed into Ox326 cells by A. Karapetyan in our lab. pAK0/Ox326A glycerol stock solution was streaked onto an Luria-Bertani Agar plate supplemented with 50 μg/mL kanamycin and 50 μg/mL ampicillin. The same

concentrations of these drugs were used in all LB media for this strain. The plates were incubated at 37°C overnight, from which a single colony was transferred to 3 mL LB medium. After shaking at 37°C, 220 rpm for 12 h, 50 µL of this culture was added to 50 mL LB in a 250 ml Erlenmeyer flask and incubated under the same conditions for 12 h. Finally, 2 mL was used to inoculate 2 L LB in a 6 L flask, which was shaken at 37°C and monitored via the optical density at 600 nm (OD_{600}). When the OD_{600} reached ~0.6, ferrous nitrilotriacetate (FeNTA) was added to a final concentration of 35 µM and IPTG (isopropylthiogalactopyranoside) was added to a final concentration of 50 µg/mL IPTG to initiate SOD overexpression. The culture was shaken at 37 °C for another 6-8 hours of until the OD_{600} reached a plateau ($OD_{600} \approx 4$).

Cells were harvested by centrifugation at 4°C, 8000 rpm for 20 min and then resuspended in cell lysis buffer. Pellets were centrifuged again under the same conditions and frozen at -20°C until needed. Frozen cell pellets were thawed on ice and resuspended in 5 mM potassium phosphate buffer, pH7.4, using 3 mL buffer for each gram of cell pellet. After that it was transferred into a homogenizer and ground into a smooth paste. Protease inhibitor (AEBSF, 4-(2-aminoethyl) benzenesulfonyl fluoride hydrochloride) and $CaCl_2$ were added to the paste to final concentrations of 0.2 mg/mL and 0.1 M, respectively. The cells were kept on ice and ruptured by sonication using 10 cycles of (30 s sonication and 30 s pause for cooling), or as needed to decrease the viscosity of the suspension. Debris was then removed by centrifugation at 4°C, 18 krpm for 30 min.

The first step of the purification was a heat cut, wherein the supernatant was brought to 0.1 M KCl by slowly adding the solid salt to the supernatant while stirring it on ice, before transferring the beaker to a water bath maintained at 60°C, for 3 min, followed by further incubation in an ice bath for 15 min without stirring. Precipitates were separated from crude Fe(Mn)SOD by centrifugation at 4°C, 18 krpm for 30 min. Ammonium sulfate was then gradually added to the supernatant while stirring on ice over a period of more

than 30 min before centrifugation again as above. The supernatant then was concentrated using an Amicon® concentrator with a 30 kDa cutoff membrane (regenerated cellulose membrane), centrifuging at 4°C, 4000 g, for 20 min intervals, until the volume was reduced to ~ 5 mL. The concentrated supernatant was loaded onto a G-25 column (Sephadex G-25 Medium), which was eluted with 5 mM potassium phosphate, pH7.4. The protein concentration in each fraction was measured at 280 nm (ε_{280} = 91900 $M^{-1}cm^{-1}$ for Fe(Mn)SOD dimers and ε_{280} = 101000 $M^{-1}cm^{-1}$ for FeSOD dimers [52]). The G-25 column was washed with 500 mM potassium phosphate buffer, pH7.4 and stored with 5 mM buffer. The fractions containing protein were combined and transfer to dialysis bags, followed by dialysis overnight at 4°C against 12 L 5 mM potassium phosphate buffer, pH7.4. The supernatant was concentrated again before loading onto a DE52 column pre-equilibrated with 5 mM potassium phosphate buffer at pH 7.4. 5 mM phosphate buffer was used to elute the Fe(Mn)SOD and fractions were collected by a fraction collector. The column was washed with 500 mM potassium phosphate buffer at pH 7.4 between uses. The protein concentration and purity of each fraction were monitored by absorbance at 280 nm and SDS-PAGE electrophoresis, respectively. Fractions containing pure Fe(Mn)SOD were pooled and concentrated to bring the protein concentration to ≈1 μM, and stored at 4°C.

2.3 Results and Discussions

2.3.1 Protein purification, metal content and activity

The SDS-PAGE shown in Figure 2-1a demonstrates the successful overexpression induced by adding IPTG to the cells. During purification process, the supernatant and pellet collected at each step were characterized by electrophoresis with the results shown in Figures 2-1b and c. It can be seen that the early fractions from DEAE-52 ion exchange chromatography contained almost no proteins other than SOD. The latter fractions contained some impurities, and therefore were not retained for characterization. MnSOD was used as control, illustrating that the overexpressed Fe(Mn)SOD and MnSOD had

same protein molecular weight on the SDS-PAGE, as expected. The non-denaturing gel in Figure 2-3 is able to resolve separate bands for MnSOD protein containing Mn, or Fe or neither[53]. It shows that the overexpressed protein is heterogeneous with respect to metal ion content, which was therefore characterized (below).

After purification, the quality of the protein was assessed via the assays summarized in Table 2-1. The extent of contamination with DNA was evaluated via the ratio of absorbances at 260 nm *vs*. 280 nm [54]. Our result is close to the value published for 100% protein (free of any DNA), that is 0.57 whereas protein containing 5% DNA (g/g) gives a high A_{260}/A_{280} ratio of 1.06[55]. It is evident that our purification procedure successfully removed DNA from the protein solution, and therefore that we can interpret A_{280} alone as a measure of protein concentration. The iron concentration was determined via the ferrozine assay, since it is more accurate than determination via the absorption at 350 nm. Using the ferrozine assay, the [Fe]/[dimer] was found to be 1.56. This is smaller than the target value of 2, the theoretical iron per dimer ratio. The specific activity of our preparations was determined using the cytochrome C assay[56]. The specific activity is much lower than that of a MnSOD control, as expected because the Fe-substituted protein has been demonstrated to be inactive in the standard assay[24]. However, the activity of 431 U/mg is much higher than Fe(Mn)SOD produced *in vitro* (≈ 100 U/mg, by unfolding and refolding with metal ion removal and replacement).

Both the specific activity and the [Fe]/[dimer] ratio implied that Mn-bound protein may present since metal binding *in vivo* exhibits only a modest selectivity[32,33,37,42]. An EPR assay[57] is used to quantify Mn and the standard curve is shown in Figure 2-2. It's found that the protein contains 3% Mn per active site Fe. However, since there is only small amount of MnSOD that is totally resistant to peroxide treatment, it should not be a big effect on our peroxidase study.

Non-denaturing polyacrylamide gel electrophoresis is used to separate and compare proteins with different mobility based on more than just the

molecular weight[58,59]. The results of non-denaturing electrophoresis through 18% polyacrylamide are shown in Figure 2-3a. We found that the Fe(Mn)SOD contains two species with similar but distinct mobilities. Earlier work by Fridovich's lab have assigned these bands to Mn_2-MnSOD (upper band, lowest mobility)[33], Mn,Fe-MnSOD (middle band) and Fe_2-MnSOD (lower band, highest mobility). We confirmed these assignments by detecting SOD activity in the gel using the NBT assay (nitroblue tetrazolium assay)[56,60]. The upper band contains almost all of the activity, as shown in Figure 2.3a. The lower two bands are attributed to Fe-bound protein as demonstrated by the iron-in-gel assay[61] and shown in Figure 2-3b.

Table 2-1 Fe(Mn)SOD protein basic characterization.

	DNA contamination	[Fe]/ [dimer]	Protein yield (mg protein/ L culture)	Specific Activity (U/mg protein)
Fe(Mn) SOD	0.56±0.07[a]	1.54±0.18[b]	26.6	431±62 U[c]

a. The DNA contamination is determined by the absorption ratio of A_{260}/A_{280}[54].
b. The dimer concentration is obtained by the absorbance at 280 nm using published extinction coefficient[56] in 50mM potassium phosphate buffer at pH7.4. The iron concentration is determined via ferrozine assay[62].
c. The SOD activity is measured using xanthine/xanthine oxidase cytochrome c method[56].

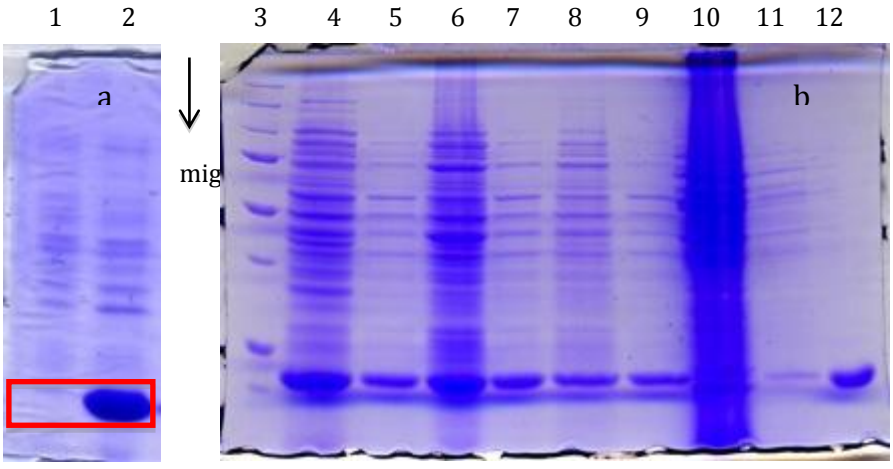

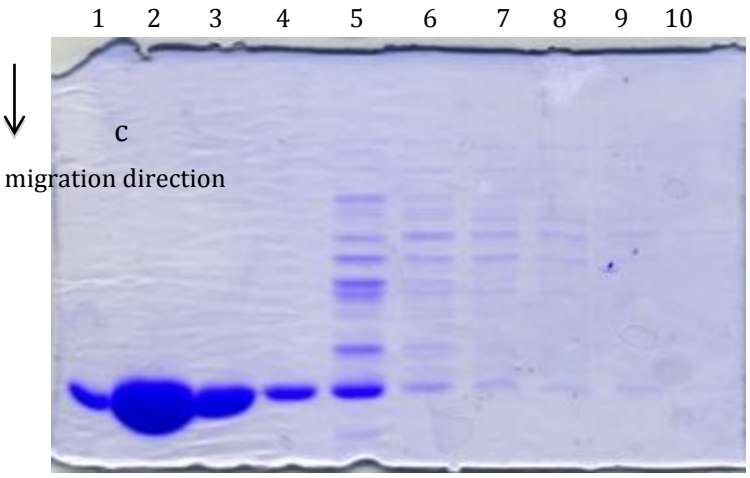

Figure 2-1 SDS-PAGE profile of Fe(Mn)SOD purification.
(a) Lane 1 and 2 are the *E. coli* cell pellet obtained from cultures without and with IPTG, respectively; Lane 3 is the pre-stained SDS-PAGE molecular weight standards (Bio-rad, 310006667); Lane 4 and 5 are the precipitate and supernatant, respectively, of centrifugation from broken cells; Lane 6 and 7 are the precipitate and supernatant after heat-cut at 60°C; Lane 8 and 9 are the precipitate and supernatant after salt-cut; Lane 10 and 11 are the precipitate and supernatant after dialysis; Lane 12 is the pure MnSOD (from lab mate Ting Wang); (b) Fractions of Fe(Mn)SOD after DEAE-52 ion exchange chromatography. (c) Non-denaturing gel electrophoresis (18% acrylamide) stained by soaking in Coomassie Blue (left) and iron in-gel-assay[61] buffer.

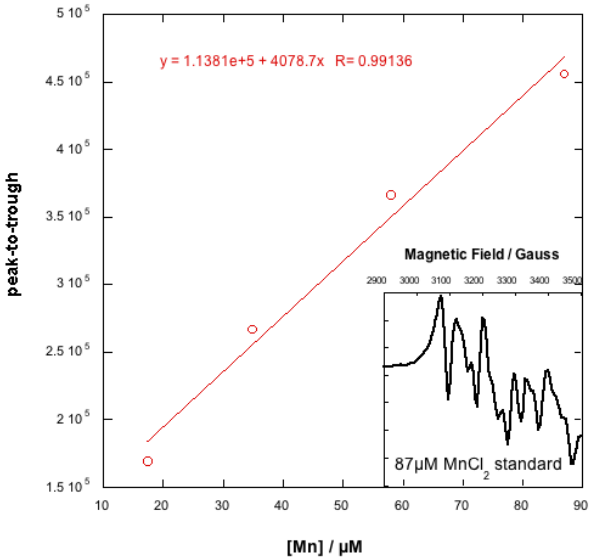

Figure 2-2 Standard curve and EPR spectrum of Mn assay.
Standard curve of EPR assay for Mn wherein the points are the signal amplitude determined from the peak-to-trough height of the third hyperfine line (inset plot).

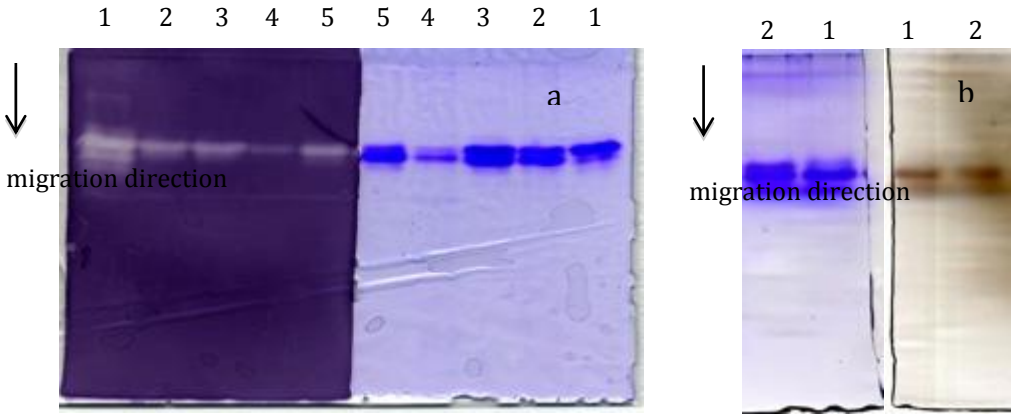

Figure 2-3 Non-denaturing polyacrylamide (18%) gel electrophoresis of Fe(Mn)SOD.
(a) Comparison of activity vs. protein content determined for two halves of the same gel cut in half, soaked in NBT buffer (left half) and Coomassie Blue (right half) and displayed as mirror images; Lane 1 was pure MnSOD from a lab mate (Ting Wang); Lane 2 and 3 were Fe(Mn)SOD overexpressed under aerobic growth conditions but purified by different methods; Lane 4 and 5 were Fe(Mn)SOD overexpressed under anaerobic growth condition purified by different methods. (b) Comparison of protein content vs. Fe content for two halves of the same gel cut in half, soaked in Coomassie Blue (left half) and iron detecting buffer (right half) and displayed as mirror images; Lane 1 and 2 were Fe(Mn)SOD overexpressed in vivo by supplemented Fe-NTA and Mn-NTA in LB media.

2.3.2 Spectroscopic characterizations of Fe(Mn)SOD

The UV-Vis absorption spectra of Fe(Mn)SOD and FeSOD were shown in Figure 2-4a for comparison, and both agree well with the earlier published work[23,33,63]. It could be seen the Fe(Mn)SOD lacked the distinguishing peak at ~350 nm that is a characteristic of Fe^{3+}SOD [52]. It also lacks the broad resonance at 478 nm that characterizes Mn^{3+}SOD.

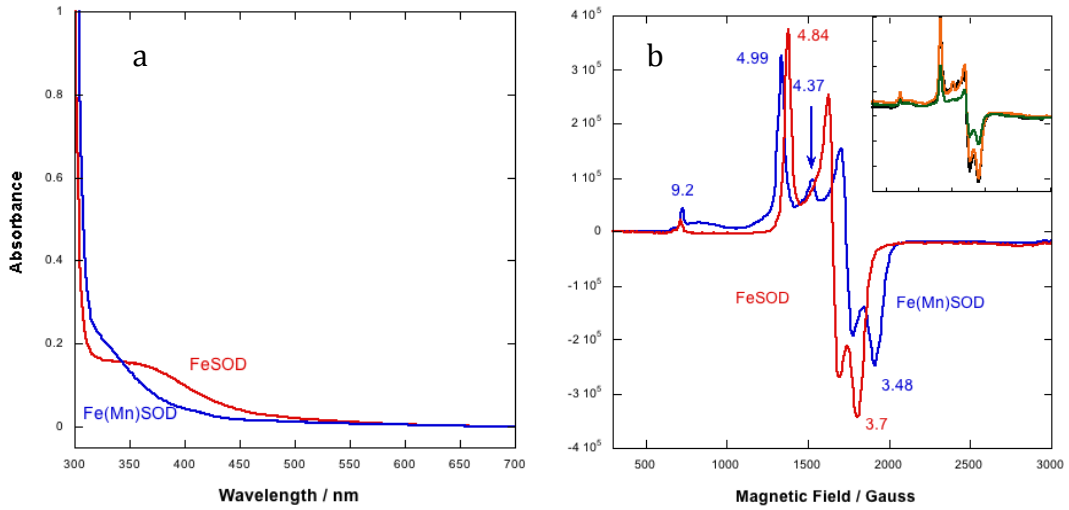

Figure 2-4 UV-Vis and EPR spectra of Fe(Mn)SOD and FeSOD.
UV-Vis (a) and EPR (b) spectra of Fe(Mn)SOD and FeSOD in 50mM potassium phosphate buffer, pH7.4. The inset plot in (b) showed the EPR spectra of three different trials.

The EPR spectra shown in Figure 2-4b were also very consistent to the previous studies[64,65], showing the signature of Fe^{3+} but not Mn^{2+}. The native enzyme exhibited a typical rhombic signal (g = 4.99 – 3.48), which arises from the middle Kramer's doublet ($m_S = \pm 3/2$) of a high-spin ferric iron[23,36], and a weak resonance signal at g = 9.2 which is characteristic of $m_S = \pm 1/2$ [66]. The inset plot in Figure 2-4b compares three different preparations, which gave pretty good reproducibility. It should be pointed out that the signal of non active site Fe (NAS Fe) [23,67] at g'= 4.37 was very small, indicating that almost the Fe in our preparations is bound in the Fe(Mn)SOD active site via this our in vivo method.

Azide and fluoride are substrate analogs that can bind to the active site Fe and give diagnostic absorption spectra. A comparison of our Fe(Mn)SOD optical signals in the presence of substrate analogs is shown in Figure 2-5a. At neutral pH, azide binding produces a strong optical absorption near 400 nm[63] (Figure 2-5a inset). The sample becomes visibly yellow because of this azide-Fe^{3+} ligand-to-metal charge transfer. Titration of the binding of azide to Fe^{3+}(Mn)SOD provides a K_d of 0.3 mM, as shown in Figure 2-5b that is also in

good agreement of the literature (0.3 mM)[36]. Binding of azide to Mn^{3+}SOD has also been characterized in previous work[68] and produces a strong CT band at 449 nm. No such band was observed.

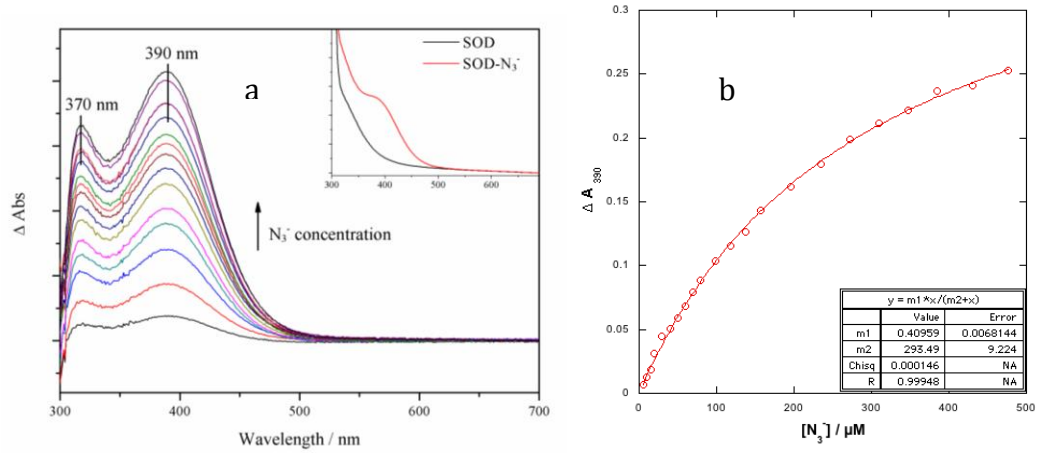

Figure 2-5 Azide binding spectra of Fe(Mn)SOD.
(a) The difference of Fe(Mn)SOD absorption of azide titration. The inset shows the overall spectra before and after azide binding. (b) Azide binding curve and the fitting line.

The pH dependence of Fe(Mn)SOD was also documented to characterize our *in vivo*-generated Fe(Mn)SOD since Fe(Mn)SOD has been found to have a much higher hydroxide binding affinity associated with a pK ≈ 6.6[63] as opposed to the pK of 9.0 that characterizes FeSOD. The spectra of our Fe(Mn)SOD at low- and high-pH, shown in Figure 2-6, agree well with those in the literature and the difference of the absorption at 370 nm provides a similar OH^- binding curve. The pKa at 6.5 is also consistent with previous studies.

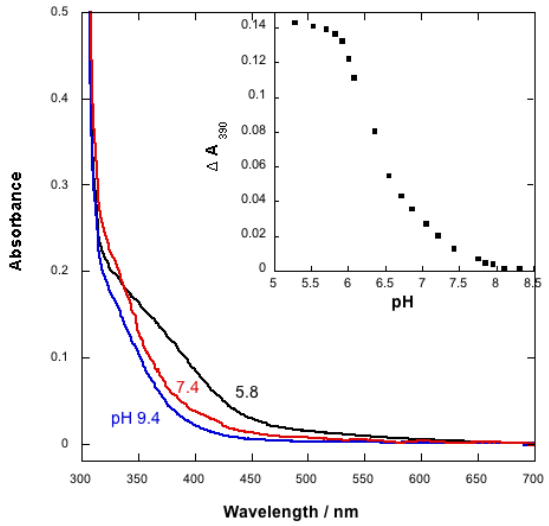

Figure 2-6 The effect of pH changes on the UV-Vis absorption of Fe(Mn)SOD.

2.4 Conclusion

The *in vivo* method we proposed generates Fe(Mn)SOD with less risk of structural perturbation by the denaturation and refolding process previously used[1,24,63]. The capture of iron binding outside the active site is also diminished as indicated by the EPR spectra. Even though MnSOD and apoprotein may also exist owing to the imperfect iron to dimer ratio, they only account for a small portion and should not have big effects on the properties of the preparation. All characterizations including EPR spectrum, azide K_d and pH titration, agree very well to the previous results for Fe(Mn)SOD, indicating the success of our enzyme expression and purification.

Chapter 3 Characterization of hydrogen peroxide treated Fe(Mn)SOD and FeSOD

3.1 Introduction

Superoxide dismutases (SOD) catalyze the disproportionation of superoxide radical ($O_2\bullet^-$), one type of reactive oxygen species (ROS) in aerobic organisms. There are three types of SOD based the protein fold and the identity of the metal ion involved in catalysis. One type of SOD employs nickel, another uses binuclear copper/zinc, and the third utilizes either iron or manganese in the active site. Although the third family includes SODs that harbor either iron (FeSOD) or manganese (MnSOD), the proteins are homologous based on their similar amino acid sequences, structures and active site geometries[20]. However, MnSOD, but not FeSOD, is the major active antioxidant enzyme in human mitochondria[26,27]. Studies on cancer have demonstrated that the loss of MnSOD and accumulation of superoxide radicals are common features of tumor cells[69]. Many cancer cells show abnormal MnSOD protein expression or catalytic activity. St. Clair and coworkers[28] proposed that imperfect MnSOD synthesis may occur due to gene mutation, short and immature mRNA transcripts or inappropriate metal incorporation. Studies on genetic regulation have indicated that the mitochondrial p53 gene is responsible for suppression of MnSOD[70,71]. Incorporation of the wrong metal ion into the active site results not only in inactive enzyme but also further damage as a result of reactive radical formation.

Recently, Yamakura [1] proposed that iron-substituted human manganese superoxide dismutase (Fe(Mn)SOD) possesses a radical-generating activity against 2,2'-azinobis-(3-ethylbenzthiazoline-6-sulfonate) (ABTS) in the presence of H_2O_2. This improper metal incorporation could occur *in vivo* since iron can compete with manganese for the metal binding site of the MnSOD polypeptide chains[32,34]. Studies have shown that when mitochondrial iron homeostasis is disrupted or when cells are short of manganese, iron accumulates and binds to MnSOD protein [29,30]. Thus, mismetallation might cause not only inactivation of MnSOD but also exacerbation of oxidative stress.

The mechanism of radical formation by Fe(Mn)SOD and H_2O_2 is unknown and complicated since FeSOD and MnSOD have different responces to peroxide treatment. FeSOD is reduced and inactivated by H_2O_2 [43-45], whereas MnSOD is generally resistant[46,47]. In the current study, we find that Fe(Mn)SOD is able to react with H_2O_2 in the absence of ABTS. The results indicated that the mechanism of this reaction is not identical to that of FeSOD. The initiation of the reaction might not be result from Fe^{3+} reduction since no Fe^{3+} signal is lost based on both optical and EPR spectra. Fluorescence spectroscopy and circular dichroism indicate that tryptophan residues are modified and local secondary structure of the enzyme is lost because of the radicals formed.

3.2 Materials and methods

Escherichia coli by carrying a plasmid-borne MnSOD gene pAK0/Ox326A were grown in LB medium supplemented with 50μg/mL kanamycin and ampicillin. To obtain Fe(Mn)SOD, ferrous nitrilotracetate (FeNTA) was added to a final concentration of 35 μM when the optical density at 600 nm reached roughly 0.6. Fe(Mn)SOD was purified essentially as previously described[52] with some modifications. The streptomycin sulfate treatment and CM column equilibration were skipped. The supernatant after ammonium sulfate cut directly run onto the G25 column, followed by dialysis against 5 mM potassium phosphate buffer at pH 7.4 for 12 h. The precipitate, if present, was removed by centrifugation at 18000 rpm before passing over the DE52 resin.

The concentration of Fe(Mn)SOD dimer [72] and ferric iron[52] were determined by the absorbance at 280 nm (ε_{280} = 9.19E4 $M^{-1}cm^{-1}$/dimer) and 350 nm (ε_{280} = 1850 $M^{-1}cm^{-1}$/dimer), respectively. The ferrozine assay [62] was used to determine the total iron concentration (Fe^{2+} and Fe^{3+}). Our preparations had 1.54 ± 0.18 equivalents of iron per dimer by this method.

Fe(Mn)SOD at 87.4 μM in 50 mM potassium phosphate buffer (pH7.4) was exposed to different concentrations of H_2O_2 (from 2.4 mM to 50.1 mM) at 25 °C. Changes in the UV-Vis spectra upon H_2O_2 treatment were determined at various times using the Cary 300- Bio UV-Visible spectrophotometer. The samples of

SODs treated with the different H_2O_2 concentrations were stored at 4°C before electrophoresis and other analyses, performed within 13 days.

Electrophoresis under non-denaturing conditions [53] was used to monitor the different forms of SOD present and assess the formation of fragments, since this method can distinguish FeSOD, Fe(Mn)SOD, MnSOD and apo-MnSOD from one-another. Gels were stained for protein with Coomassie blue G-250.

The coordination geometry of ferric iron in the active site was characterized by EPR using a Bruker 300MX spectrometer. EPR spectra were collected at 9.32 GHz at 130 K, with 200 mW nominal microwave power, 10 G modulation amplitude. EPR spectra were collected of the same samples of H_2O_2-treated Fe(Mn)SOD as were used for UV-Vis measurements, to characterize the time course of reactions. 100 μL aliquots were mixed with equal volume of glycerol and frozen in liquid N_2.

Circular Dichroism (CD) was used to monitor secondary structure and tryptophan residues of Fe(Mn)SOD, to learn what changes occured upon H_2O_2 treatment. All CD spectra were acquired on a Jasco J-815 spectrometer with a 1 mm path length quartz cuvette. Proteins were dissolved to a concentration of 4 μM in 50 mM phosphate buffer at pH 7.4. Wavelength scans were conducted using a 0.5 nm step size and a speed of 2 nm/s from 190 to 260 nm. Background scans without enzymes were also obtained and subtracted from the wavelength scans prior to converting millidegrees to mean per-residue ellipticity (θ).

3.3 Results

Reaction between Fe(Mn)SOD and H_2O_2

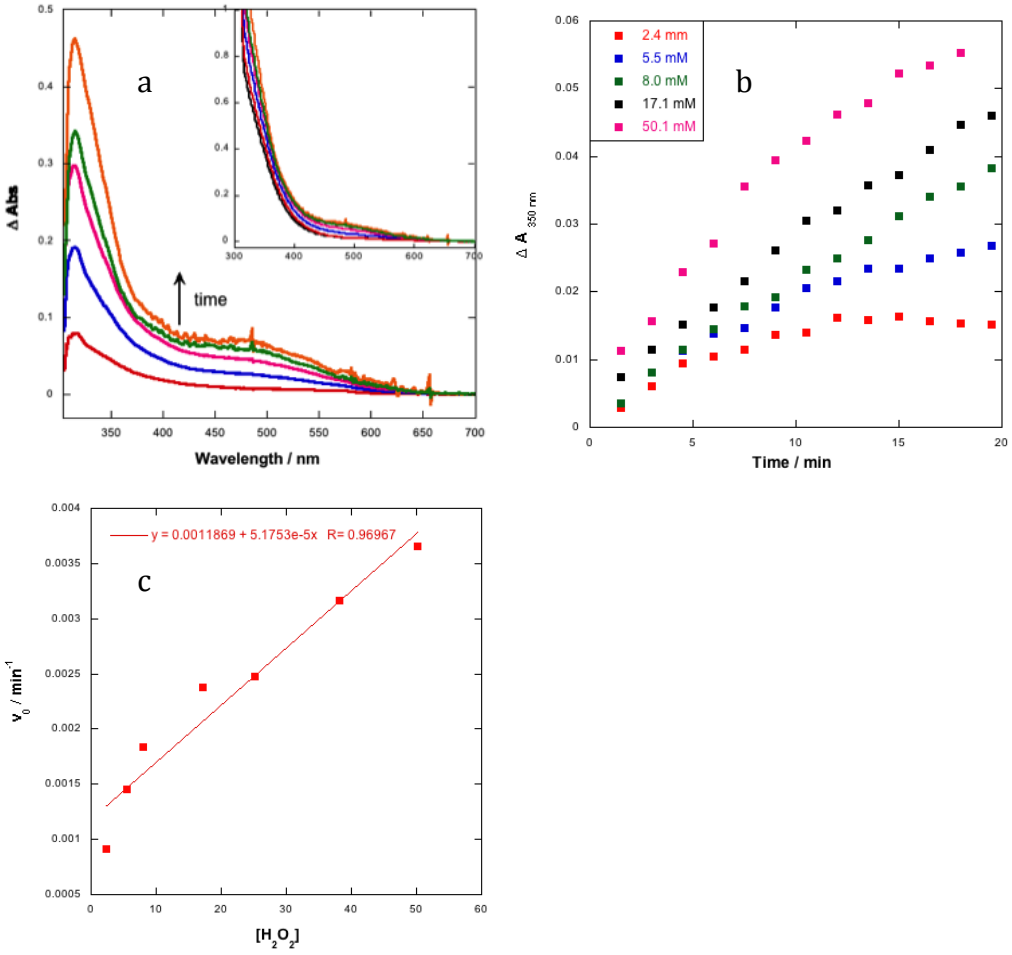

Figure 3-1 UV-Vis spectra of Fe(Mn)SOD upon H_2O_2 treatment.
(a) The time-dependent difference spectra of Fe(Mn)SOD's UV-Visible signal upon H_2O_2 treatment. The active site [Fe] =1 mM in 50 mM potassium phosphate buffer, pH7.4, and the H_2O_2 concentration was 59.7 mM. The reaction was conducted in a 2mm path length cuvette and the t=0 spectrum was subtracted from each spectrum for the main panel. Aliquots were taken at different times to prepare EPR samples. The inset plots the observed spectra at 5 min (red), 10 min (blue), 15 min (hot pink), 25 min (green), and 40 min (orange), respectively. (b) The time-dependence change of absorbance at 350 nm treated with different amount of H_2O_2. Protein dimer is 87.4 μM in 1 cm path length cuvette. (c) The initial rate of Fe(Mn)SOD exposing to different H_2O_2 concentration.

Fe(Mn)SOD enzyme overexpressed from *E. coli* at pH 7.4 displays a characteristic absorbance extending to 450 nm but lacking the distinct maximum absorption at 350 nm of FeSOD [52]. The optical spectrum of Fe(Mn)SOD grew in

amplitude and developed a new feature at 315 nm and a broad maximum centered near 485 nm upon H_2O_2 treatment, as illustrated in Figure 3-1a for spectra collected as a function of time. The feature at 315 nm is attributable to the oxidation of tryptophan residues [73,74]. The shoulder peak at ~500 nm has never reported for H_2O_2-treated FeSOD or Cu,ZnSOD. However similar absorption at 520 nm was reported [66,75] for Fe^{3+}-EDTA upon addition of H_2O_2 and was ascribed to a peroxide-to-iron ligand-to-metal charge transfer (LMCT) transition. It can be seen from Figure 3-1b that the rate of growth of the signal at 350 nm depends on the H_2O_2 on concentration. The more H_2O_2 was added, the faster the peak grew. The rate vs. [H_2O_2] is added in Figure 3-1c. It looked like first order reaction in H_2O_2 except a poor R square value. That's because of the formation of oxygen gas during the reaction. The increased H_2O_2 concentration produced more oxygen gas. When the O_2 concentration was above the solubility, oxygen bubbles were seen coming out from the solution. The absorptions were less accurate owing to the impact bubbles.

Protein secondary structure change based on Circular Dichroism

To determine whether exposure to H_2O_2 brought about a change in the secondary structure of Fe(Mn)SOD, far-UV CD (240 – 190 nm) was used [76] and the spectra were shown in Figure 3-2. The native enzyme displayed typical absorption for α-helices [77-79], indicated by the negative ellipticity at 227 and 208 nm, and positive ellipticity at 193 nm. Upon H_2O_2 treatment, the absolute ellipticities at 193, 208 and 227nm all decreased indicating a loss of α-helices. A shift in the maximum from 208 nm shifted to 204 nm accompanied the increased ratio of ellipticities at 208 and 227 nm as the concentration of H_2O_2 used increased. Previous work found that a shift from 208 nm to higher frequencies was associated with destabilization of α-helices, probably because of the formation of shorter peptide chains [80].

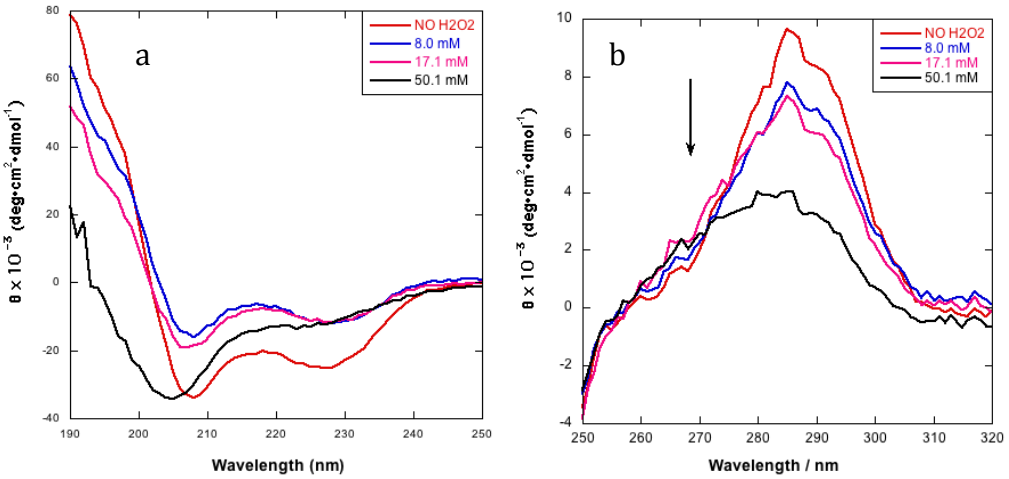

Figure 3-2 Circular Dichroism spectra of Fe(Mn)SOD treated with different concentration of H_2O_2.
Far-UV (a) and near-UV (b) CD spectra of Fe(Mn)SOD treated with different concentration of H_2O_2. Samples contained ~4μM and 80μM protein dimer for far- and near-UV measurement, respectively, in 50mM potassium phosphate buffer, pH7.4 at 25 °C.

The CD in the near-UV region of protein spectra arises from aromatic side chains (phenylananine, tyrosine, and tryptophan) and disulfide bonds [81,82] and provides very useful information on changes in the environment nearby. As shown in Figure 3-2b, the ellipticity around 280 nm, which is characteristic of Trp side chains [83], was obviously lost upon H_2O_2 treatment. Both far- and near-UV CD observations suggest that the modification and probably loss of Trp residues upon exposure to H_2O_2, leads to the formation of less stable α-helices [79].

In contrast, H_2O_2-treated FeSOD exhibited negligible change to its CD spectra in response to treatment with H_2O_2, as indicated in Figure 4-2. This is evidence that FeSOD undergoes more subtle modification upon H_2O_2 treatment compared to changes affecting Fe(Mn)SOD, which is consistent to Yamakura's results [44]. He found that the H_2O_2-treated FeSOD exhibited similar spectra to the native enzyme using far-UV CD, concluding that H_2O_2 might modify the amino acid residues but not change the gross conformational.

Large-scale structural changes affecting electrophoretic mobility

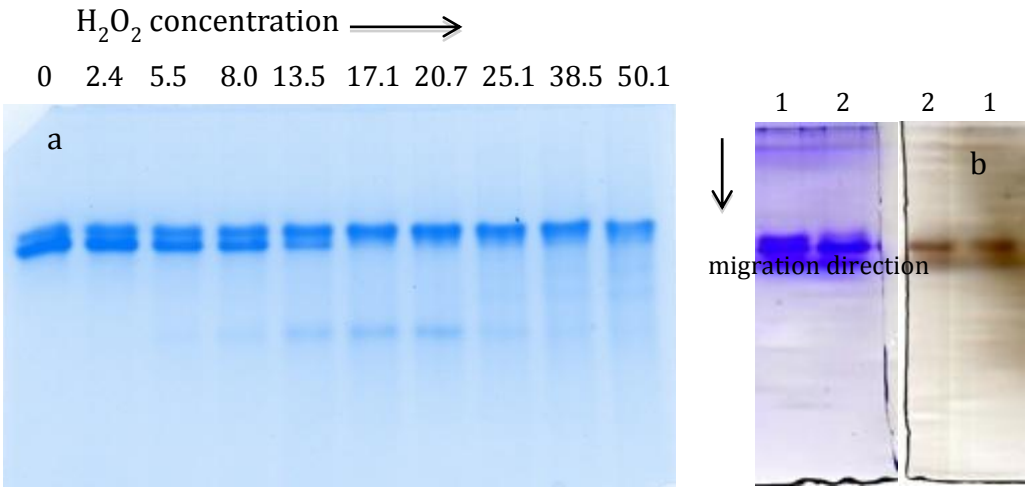

Figure 3-3 Native gel electrophoresis of Fe(Mn)SOD samples treated with different amounts of H_2O_2.
(a) Native gel electrophoresis of Fe(Mn)SOD samples treated with different amounts of H_2O_2. The concentration of each sample was listed on top of the gel from 0 to 50.1 mM. Each lane contained ~12 μg of protein. The gel was 18% acrylamide and was stained with Coomassie Blue R-250. (b) Comparison of protein content vs. Fe content for halves of the same native gel cut in half soaked in Coomassie Blue (left half) and iron detecting buffer (right half) and displayed as mirror images; Lane 1 and 2 were Fe(Mn)SOD overexpressed under anaerobic and aerobic growth conditions.

Non-denaturing electrophoresis has been used to resolve SOD species containing different stoichiometries and identities of metal ions[58,59,61]. It has also been used to distinguish different oligomeric states of proteins. Fe(Mn)SOD is seen to comprise two populations, based on non-denaturing electrophoresis, The faster migrating band corresponds to Fe-containing protein as shown in Figure 3-3b whereas the more slowly migrating band corresponds to apoprotein or Mn-bound protein[32,34,38]. Upon H_2O_2 treatment, we found that the lower band disappeared before the upper band and a new species was formed in concert with loss of the lower band, as exhibited in Figure 3-3a. The new band was only formed at intermediate concentrations of H_2O_2 and was replaced by a diffuse smear of protein migrating somewhat faster than the main bands, upon treatment with higher concentrations. The reason for this is not clear and it might due the high tendency of diffusion of the produced reactive intermediate.

Yamakura [44] studied the mobility of H_2O_2-inactivated FeSOD from Pseudomonas and the polyacrylamide gel electrophoresis displayed some minor slower-moving protein bands with no change in the mobility of the major protein bands. He proposed that inactivated FeSOD only underwent only subtle changes in some amino acid residues and did not suffer gross conformational change.

Tryptophan Fluorescence

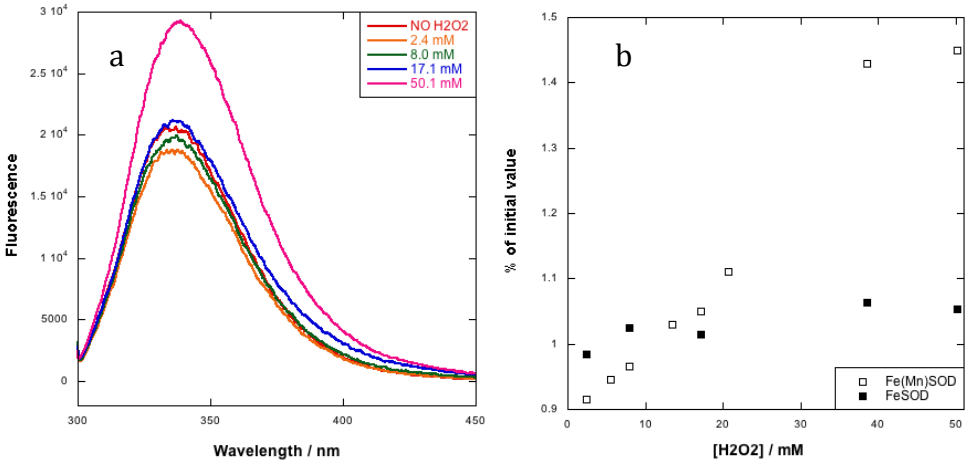

Figure 3-4 Fluorescence emission spectra of recorded for Fe(Mn)SOD treated by different H_2O_2 concentration.
Samples contained ~4 μM protein in 50 mM potassium phosphate buffer, pH 7.4 at 25 °C and excited at 295 nm. (b) Influence of hydrogen peroxide concentration on the tryptophan fluorescence of Fe(Mn)SOD and FeSOD. Relative fluorescence intensity is taken by dividing individual fluorescence to those of native protein.

Tryptophan fluorescence is a sensitive probe for detecting changes in the local environment surrounding the indole ring [84,85]. The emission spectra of Fe(Mn)SOD treated with H_2O_2 are shown in Figure 3-4a. It can be seen from Figure 3-4b that at low H_2O_2 concentrations, the fluorescence was lost as we expected[86], indicating that Trp residues are modified. However, when higher H_2O_2 concentrations were used the fluorescence increased. Considering the many factors that govern quenching of protein fluorescence, we propose that the increase in fluorescence might be attributable to diminished quenching by Fe upon Fe's release by the peroxide treatment. It has been shown that binding of Fe resulted strong quenching of fluorescence [87-90]. The iron in-gel electrophoresis[61] (shown in Figure 4-7) did indeed indicate that more Fe was lost as the concentration of H_2O_2 was increased.

Effect of H_2O_2 treatment on the Fe site, based on EPR spectra of Fe(Mn)SOD

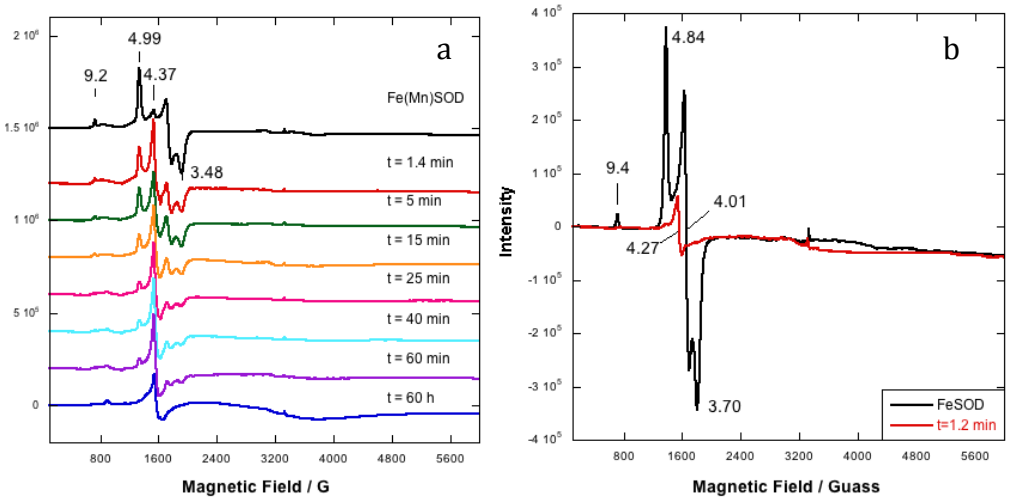

Figure 3-5 Effect of duration of treatment on EPR spectra of Fe(Mn)SOD and FeSOD upon treatment with H_2O_2.
EPR spectra of Fe(Mn)SOD (a) and FeSOD (b) upon treatment with 30 mM H_2O_2. Samples contained 0.5 mM Fe(Mn)SOD on the basis of active site Fe. This was dissolved in in 50 mM potassium phosphate buffer, pH7.4. At the stated time 100 µl of the SOD solution was removed from the reaction, augmented with 100 µL glycerol and frozen in liquid N_2. Samples were observed at 130 K. The g' values of predominant spectral signals are indicated.

Studies of EPR spectra can provide information of the environment of the paramagnetic iron center in the active site of Fe(Mn)SOD[64,65]. The time course EPR spectra of H_2O_2-treated Fe(Mn)SOD are displayed in Figure 3-5. The native enzyme exhibited a typical rhombic signal (g = 4.99 – 3.48), which arisen from the middle Kramer's doublet (Ms = ±3/2) of a high-spin ferric iron[23,36], and a weak resonance signal at g = 9.2 are characteristic of Ms = ±1/2 [66]. It should be noted that the Fe(Mn)SOD prepared by our in vivo method contained small amount of non active site iron (NAS Fe) [23,67], indicated by the tiny signal at g = 4.3 of native protein. The absence of NAS Fe minimized the effect of metal-derived contributions to our result.

Upon H_2O_2 treatment, the EPR signal of Fe(Mn)SOD exhibited a more rhombic symmetry (Figure 3-5a). As indicated by Figure 3-6a, there was 30-40% signal loss. Thus it appears that most of the Fe remains in the 3+ state. By comparison, more than 90% of the ferric ion in FeSOD was lost within ~1.2 min

and only a small amount of NAS Fe remained visible after exposure to H_2O_2, (Figure 3-5b). This demonstrates that FeSOD is rapidly reduced by H_2O_2 in agreement with the results of UV-Vis absorption studies [43,91]. It also suggested that the reaction of H_2O_2 with Fe(Mn)SOD did not follow the same mechanism as the reaction with FeSOD. For Fe(Mn)SOD, the H_2O_2 treatment has a reversible effect only, as addition of azide (N_3^-) produces the same EPR signal after 12 hours' reaction with H_2O_2 as is produced by addition of N_3^- to untreated Fe(Mn)SOD (Figure 4-4), displaying the same rhombic EPR signal [23,36] (g = 4.28) indicative of near-octahedral geometry and thus a six-coordinated Fe^{3+} complex. Moreover the presence of N_3^- is known to suppress effects of H_2O_2 on Fe(Mn)SOD suggesting that the form that interacts with the active site is most likely HO_2^-, which had low binding affinity compared to azide anion[43]. Thus we propose that the 'new' rhombic species that appears as early as 1.4 minutes into treatment does not represent Fe loss from the active site, but rather formation of a 6-coordinate adduct of HO_2^- to Fe^{3+} in Fe(Mn)SOD. It's also found that the addition of azide could affect the response of Fe(Mn)SOD to H_2O_2. As shown in Figure 4-8, small bleaching of SOD-N_3 complex was seen in the UV-Vis spectra and no further decrease in 340nm because of Trp oxidation. The CD data also proved that structural changes were much less obvious in the presence of azide. The suppression dissolved oxygen generation by azide further indicated that azide is a more competitive binding analog than HO_2^- that will inhibit H_2O_2 reaction because of blocking the active site.

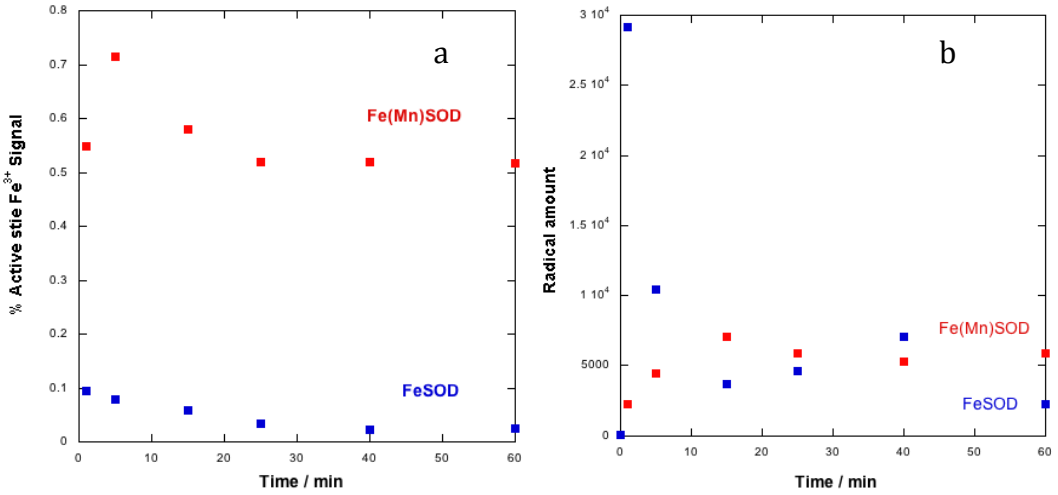

Figure 3-6 Double integration of EPR signal of Fe(Mn)SOD and FeSOD after H_2O_2 treatment.
(a) The high spin ferric EPR signal of Fe(Mn)SOD and FeSOD after H_2O_2 treatment as percentage of native protein. The amounts of ferric signal were obtained by double integration of the EPR spectra. (b) Comparison of radical production at g' = 2 of H_2O_2-treated protein. The radical amounts were obtained by double integration.

Direct observation of radical species formed upon exposure to H_2O_2

EPR signals of free radicals were evident at g = 2 for both H_2O_2 treated Fe(Mn)SOD and FeSOD. This are most likely due to aromatic radicals on the basis of chemical stability arguments, since none of our samples were quenched rapidly, so only long-lived radicals could be trapped. However, our observation temperature makes it hard to identify the exactly type of radical and hyperfine structure [92,93], since Trp radicals are broadened upon freezing.

While both Fe(Mn)SOD and FeSOD exhibited radicals upon treatment with H_2O_2, both the quantity and time course were different. For FeSOD, the sample collected after 1.2 minutes of treatment displayed the maximum radical intensity (Figure 3-6b) and the radical concentration decayed rapidly thereafter. However, H_2O_2-treated Fe(Mn)SOD displayed a maximum concentration of radicals 15 minutes into the treatment and a much slower decay time. This indicates that either Fe(Mn)SOD sustains continuous radical production that compensates for radical decay, or the radicals have a longer life time.

3.4 Discussions

The peroxidase activities of Cu,ZnSOD and FeSOD have been well studied and the mechanisms substantially agreed-upon. It's widely accepted that the initial step is fast reduction of Cu^{2+} or Fe^{3+} by HO_2^-, followed by reaction between Cu^+ or Fe^{2+} and a second equivalent of HO_2^- generating a bound oxidant. Amino acid residues, especially Trp, Tyr or His, close to the metal active site were oxidized by this bound oxidant and the enzyme inactivated[43,45,74,91,94-99]. Exogenous alternative substrates could also be oxidized instead of amino acid residues, and the presence of these sacrificial substrates protected the enzyme from inactivation [74,96]. Large molecules with limited access to the oxidant were not oxidized, but when bicarbonate was present it was able to mediate their oxidation by acting as an intermediary diffusible radical oxidant [100]. It was therefore proposed that the peroxidase activities of Cu,ZnSOD and FeSOD were based on Fenton chemistry mediated by Cu^{2+} or Fe^{3+}, respectively [101,102]. However, our results find that the protein context is very important too. Even though Fe^{3+} was bound in the active sites of both Fe(Mn)SOD and FeSOD, the reaction between Fe(Mn)SOD and H_2O_2 was very different from that of FeSOD, and the two systems appear to follow different mechanisms.

The UV-Visible spectra of H_2O_2–treated FeSOD shown in Figure 4-1a show that bleaching at 350 nm occurred immediately upon exposure to H_2O_2 and indicate reduction of Fe^{3+} to Fe^{2+}, followed by Trp oxidation. The reaction between H_2O_2 and Fe^{3+} is a 1:1 stoichiometric reaction according to previous observations [43,45,91] and only Fe^{3+} reduction was observed at low H_2O_2 concentration, as shown in Figure 4-1b. Trp oxidation occurred probably at higher H_2O_2 concentration. In contrast, the Fe(Mn)SOD was not significantly reduced upon H_2O_2 treatment based on both the optical and EPR spectra. Instead it displayed a gradual increase in absorbance in 300–550 nm.

The growing peak at 315 nm was attributed to the oxidation of Trp residues, consistent with the fact that it occurred for both proteins. However, this oxidation rate depended on H_2O_2 concentration in the case of Fe(Mn)SOD.

For the FeSOD, this oxidation occurred rapidly for the first 1-2 minutes and then stopped. This was probably because of protein inactivation based on our data in Figure 3-6, and consistent with prior work [94,95].

Fe(Mn)SOD also appeared resistant to inactivation by H_2O_2 on the basis of SOD activity measured using the cytochrome C assay as well as the nitrobluetetrazolium photochemical method[56] (Figure 4-5). However, these activities can be explained on the basis of the presence of Mn in some ~3% of the active sites as determined by the EPR manganese assay. The presence of MnSOD was very difficult to avoid due to the *in vivo* competition between Fe and Mn[32,33]. Since MnSOD is known to be resistant to H_2O_2 [45] the retained activity is simply a reflection of this population present in our preparations of Fe(Mn)SOD, and has a very small contribution to our results due to the small magnitude of this contamination and the fact that it is known to not undergo changes upon treatment with H_2O_2. Similarly, the EPR signals we observe are due exclusively to Fe and therefore are not subject to complication by Mn-containing sites. Our finding that no Fe^{3+} reduction occurred in H_2O_2-treated Fe(Mn)SOD based on UV-Vis spectra was consistent with the EPR spectra.

The EPR spectra also revealed a change in the coordination environment of Fe^{3+}. Because the change was fully reversible we conclude that Fe was not released from the active site. Thus our data demonstrate that active site Fe^{3+} becomes six-coordinate, which is most simply interpreted as formation of a complex with H_2O_2 bound to Fe^{3+}, as the Fe^{3+} became more rhombic without obvious loss of high spin ferric iron signal overall. In comparison, the EPR spectrum of FeSOD lost most of its high spin iron signal and the residual signal can be attributed to the NAS Fe. The fundamental difference between the reactions of the Fe ions of Fe(Mn)SOD and FeSOD is consistent with their different reduction potentials. The lower potential of Fe(Mn)SOD makes it more difficult to reduce, and our results indicate that indeed H_2O_2 is unable to do so. Any reactions that follow must therefore be interpreted as the result of chemistry that does not follow the canonical Fenton mechanisms, since there rely on the presence of reduced metal ion as an electron donor to H_2O_2.

The effect of H_2O_2 treatment on secondary structure of the protein was also studied by CD spectroscopy. As indicated in Figure 4-2, the secondary structure of H_2O_2-exposed FeSOD was retained and in good agreement with previous results[44,45]. This was different from those of H_2O_2-treated Fe(Mn)SOD, which not only displayed loss of near-UV Trp signal, but also changes of α-helices in far-UV region.

The mechanism of H_2O_2 inactivated FeSOD has been widely studied even though clarified yet. One of the most popular hypotheses is that the present of Trp residue contributes to the enzyme inactivation. The lost of Trp at some exact sites leads to the resistance of H_2O_2 [35,86,103]. The significance of Trp residues has been well accepted not only for H_2O_2-treated FeSOD but also for Cu, Zn-SOD. However, the exact site of the functional Trp is not consistent. Some proposed that the Trp near the active site is accountable for the inactivation while some assume the Trp on the protein surface is involved [74]. Another more reasonable explanation is that the reaction of H_2O_2 and Fe at the active site generates a highly active oxidant. This reactive species, probably $OH^{\bullet}$ will oxidize the Trp residues near the active site, or oxidize the external substrate with the help of bicarbonate diffusion.

Chapter 4 Supporting Information: Characterization of hydrogen peroxide treated Fe(Mn)SOD and FeSOD

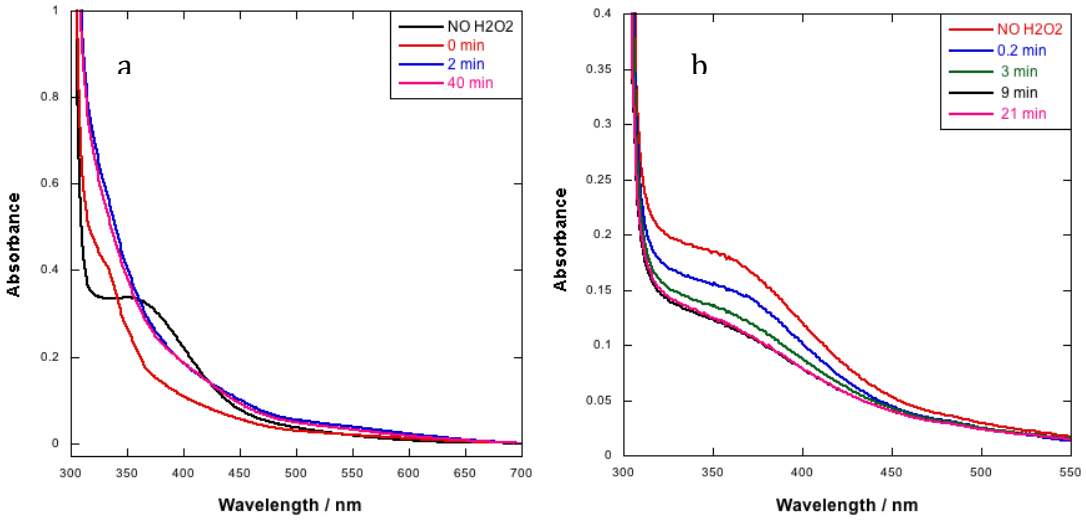

Figure 4-1 The time-dependent UV-Visible spectra of FeSOD upon H_2O_2 treatment. (a) The active site [Fe] =1 mM in 50 mM potassium phosphate buffer, pH7.4, and the H_2O_2 concentration is 59.7 mM. The reaction was conducted in a 2 mm path length cuvette. Aliquots were taken at different times to prepare EPR samples. (b) Sample contained 87.4 μM protein (dimer) and 0.24 mM H_2O_2. The reaction was running in 1 cm path length cuvette.

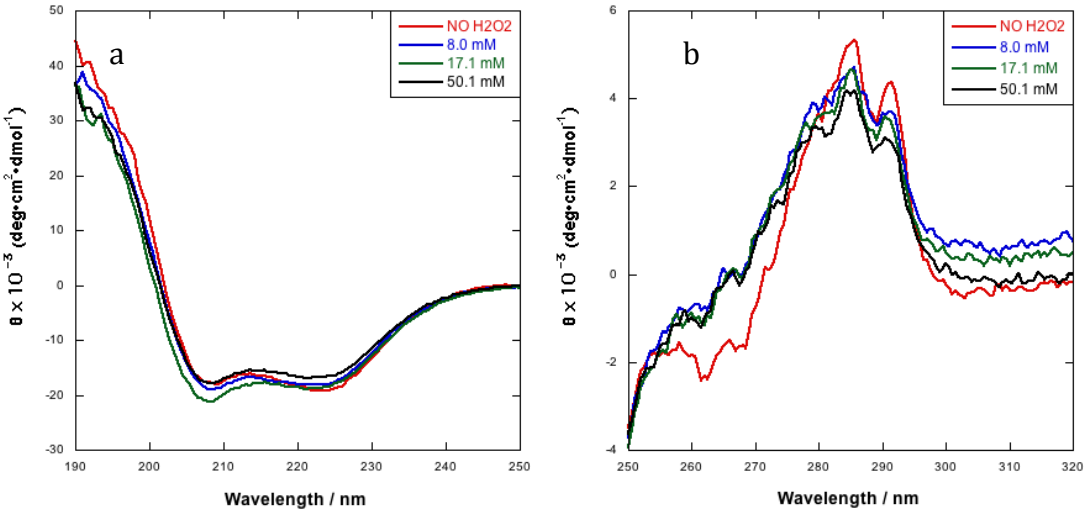

Figure 4-2 Circular Dichroism spectra of FeSOD treated with different concentration of H_2O_2.
Samples contained ~4 μM and 80 μM protein dimer for far- and near-UV measurement, respectively, in 50 mM potassium phosphate buffer, pH7.4 at 25 °C.

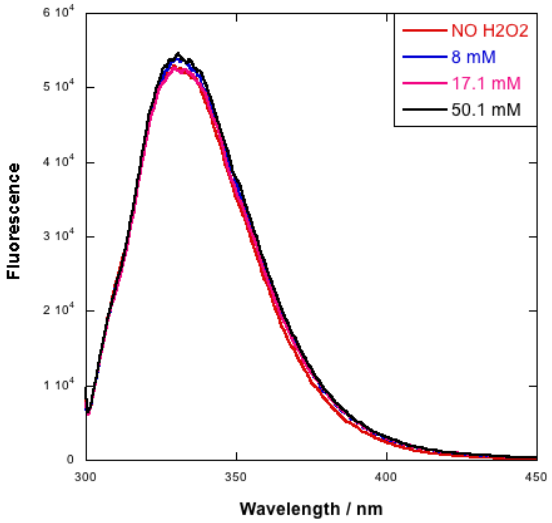

Figure 4-3 Fluorescence emission spectra recorded for FeSOD treated by different hydrogen peroxide concentration.
Samples contained ~4 µM protein in 50 mM potassium phosphate buffer, pH 7.4 at 25 °C and excited at 295 nm.

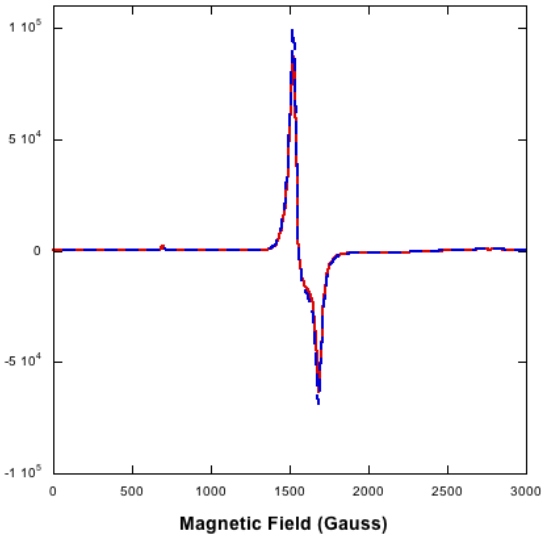

Figure 4-4 The effect of azide binding on the EPR spectra of Fe(Mn)SOD active site. The protein pretreated with H_2O_2 for 12 h before binding to azide was shown in red and the protein bound to azide before H_2O_2 treatment for 12 h. Samples contained 0.5 mM active site Fe in 50 mM potassium phosphate buffer, pH7.4 at 130 K and glycerol was added to a final concentration of 50% v/v. The concentration of hydrogen peroxide and sodium azide were 29.7 and 5 mM, respectively.

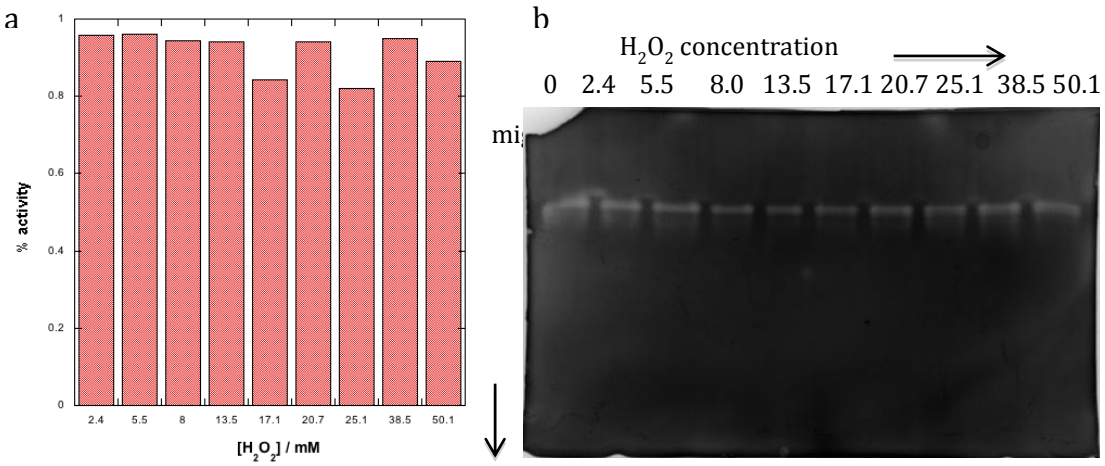

Figure 4-5 Activities of H_2O_2-treated Fe(Mn)SOD.
(a) Residual activity of Cytochrom C Assay of individual sample exposed to different H_2O_2 concentration compared to native enzyme. (b) Non-denaturing gel soaked in NBT buffer.

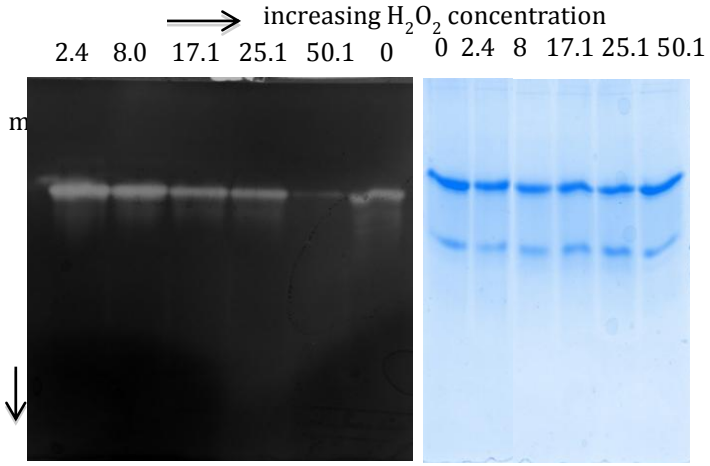

Figure 4-6 Non-denaturing gel of FeSOD protein treated with different amount of H_2O_2.
Left panel was soaked in NBT buffer and right panel was in Coomssie Blue R-250. The concentrations of H_2O_2 were listed on top of the gel.

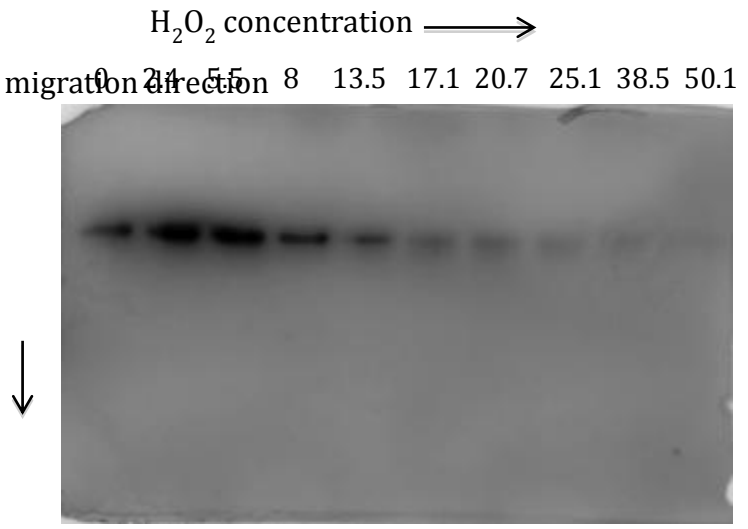

Figure 4-7 Iron-in-gel assay for Fe(Mn)SOD treated with different concentration of H_2O_2.
The concentrations of H_2O_2 were listed on top of the gel.

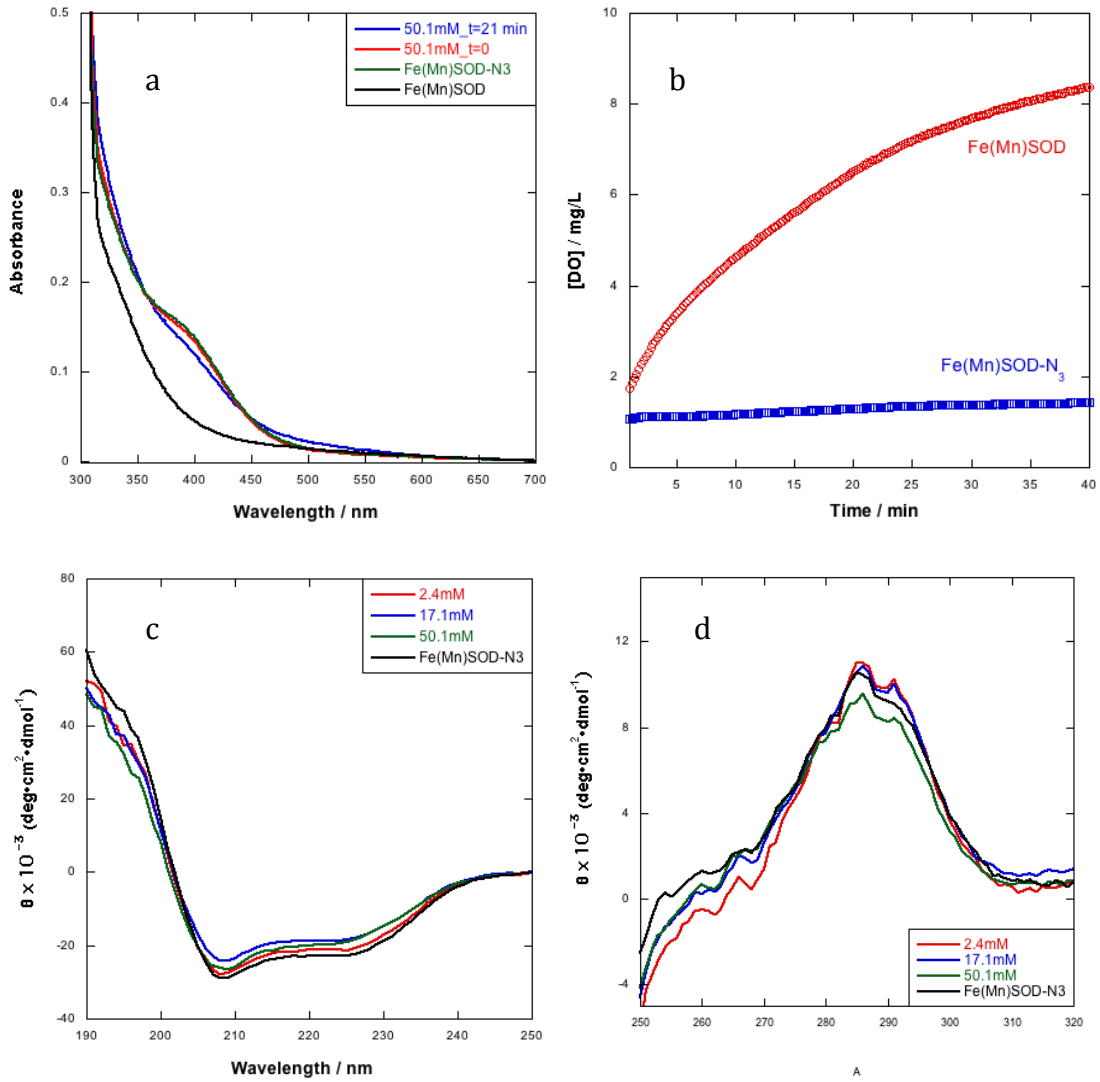

Figure 4-8 The effect of azide binding on Fe(Mn)SOD upon H_2O_2 treatment. (a) The UV-Visible spectra of native Fe(Mn)SOD, SOD-N_3 complex, and SOD-N_3 treated by 50.1 mM H_2O_2 at t = 0 and t = 21 min. Sample contained 69.7 μM protein (Fe active site) and azide concentration was 0.47 mM. (b) The production of dissolved oxygen upon 0.75 mM H_2O_2 treatment with and without aziding. The Fe(Mn)SOD dimer and azide concentrations were 11.2 μM and 100 μM. Far UV (c) and near UV (d) CD spectra of Fe(Mn)SOD treated with different concentration of H_2O_2 in the presence of azide. Samples contained ~4 μM and 80 μM protein dimer for far- and near-UV measurement, respectively, in 50 mM potassium phosphate buffer, pH7.4 at 25°C. The azide concentration was 23.5 μM.

Chapter 5 Chapter four: Peroxidase Activity Comparison between Fe(Mn)SOD and FeSOD based on ABTS and Amplex Red Assays

5.1 Introduction

It has been a long time since the proposed peroxidase activity of Cu, Zn-SOD and the studies of its mechanism were reviewed by Fridovich in 2010[97,98]. A classic mechanism proposed that a fast reversible reduction of Cu(II) to Cu(I) by HO_2^- (active species of H_2O_2) generated a bound oxidant, probably SOD-Cu(II)-OH, or SOD-Cu(III), or SOD-Cu(I)-HO_2^-. Small substrates that had access to the solvent channel, or the amino acid residues close to the active site could be oxidized[104-106]. Large substrate molecules could be oxidized in the presence of HCO_3^- /CO_2, as carbonate radical ($CO_3^{\bullet-}$) could be formed in the active site and diffuse into the bulk solution where it could oxidize other species[74,99,107]. In contrast, if Cu, Zn-SOD's own amino acid residues were oxidized by the active site oxidant, the enzyme was inactivated and Cu could be released into solution where it could catalyze other oxidative reactions. However the presence of superoxide analogs, such as azide, could protect the protein from deactivation, indicating that HO_2^- must gain access to a site in Cu's coordination sphere in order to react.

FeSOD was also found to react with H_2O_2, becoming inactivated. The mechanism is not as clear as in the case of Cu, Zn-SOD but is believed to follow the same general sequence of events based on the results as follows. Initially, Fe(III) is rapidly reduced to Fe(II) by H_2O_2, then the Fe(II) reacts with H_2O_2 yielding an oxidant that would oxidize the amino acid residues and deactivate the protein[43-45,86,91,95]. However, the oxidation of alternate substrates by the oxidant of FeSOD has not been reported.

$$Fe^{3+} + HO_2^- \rightarrow Fe^{2+} + O_2^{\bullet-} + H^+$$

$$Fe^{2+} + H_2O_2 \rightarrow OH^- + [(Fe^{3+} + {}^{\bullet}OH) \Leftrightarrow (Fe^{4+} = O + H^+)]$$

In last chapter, H_2O_2-treated Fe(Mn)SOD was demonstrated to react different with H_2O_2 than compared to FeSOD, in not undergoing metal ion reduction, but instead displaying altered active site coordination geometry and

secondary structure. However, FeSOD and Fe(Mn)SOD did have similar features such as the formation of a radical intermediate and its capabilities to oxidize amino acid residues.

As proposed by the peroxidative mechanism of Cu, Zn-SOD, the presence of alternative substrates could be oxidized instead of amino acid residues. In Yamakura's paper[1], the possible toxicity of Fe(Mn)SOD was demonstrated via the ABTS assay and it was hypothesized that the fact that Fe(Mn)SOD could oxidize ABTS should be interpreted as evidence that it could generate hydroxide radical ($OH^{\bullet}$), which was proposed to be the active species that reacted with ABTS. However, there was not strong evidence for $OH^{\bullet}$ formation and the mechanism of oxidation of ABTS by Fe(Mn)SOD remains opaque. As part of our investigation of the mechanism of reaction between H_2O_2 and Fe(Mn)SOD, we now seek to clarify events leading to the oxidation of ABTS by Fe(Mn)SOD.

5.2 ABTS assay

2,2'-azinobis-(3-ethylenzthiazoline-6-sulfate) (ABTS) is a useful chromogenic probe because it is converted to an intense green chromophore upon reaction with one-electron oxidants. ABTS is widely used for assaying peroxidases[108-110] because it can serve as the sacrificial electron donor and the resulting product is easily quantified based on its absorbance with broad maxima at 415, 650 and 732 nm [111,112]. The structure of $ABTS^{\bullet+}$ is shown in Figure 5-1. The absorbance at 415 nm was the strongest one, with an extinction coefficient of 36 $mM^{-1}cm^{-1}$[100]. Similarly, $OH^{\bullet}$ was proposed to react with ABTS to generate a relatively stable $ABTS^{\bullet+}$ in a diffusion-controlled reaction, based on pulse-radiolysis[113]. Recent studies also proved that not just $OH^{\bullet}$ but also many other powerful oxidants such as Fe (VI) and other enzyme intermediates could oxidize ABTS to the chromophoric cation radical[114,115].

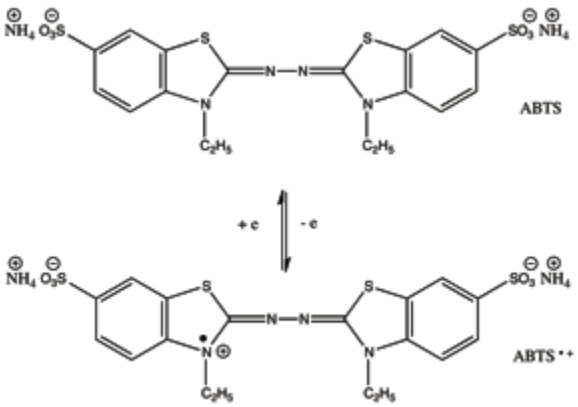

Figure 5-1 Structures of ABTS and ABTS$^{\bullet+}$.

5.2.1 Materials and experiment

ABTS was obtained from Sigma Co. (30931-67-0) and 35% aqueous solution of hydrogen peroxide (H_2O_2) was obtained from Mallinckrodt Chemicals. The deionized (DI) water used in all the experiments was purified using a Millipore Milli-Q Plus System. ABTS was dissolved in deionized water to make 0.1 M stock solution and then stored at 4°C in the dark using Amber tube[111]. The concentration of ABTS solution was determined using a 5000-fold dilution at 340 nm (ε_{340} = 36.6 $mM^{-1}cm^{-1}$[100]) by UV-Vis spectroscopy. The spectra of ABTS and ABTS$^{\bullet+}$ after oxidation by enzyme were shown in Figure 4-1. EDTA solution was added to bind to metal cations with a final concentration of 0.2mM as suggested in Yamakura's work[1]. Fe(Mn)SOD was diluted in 50 mM potassium phosphate buffer, pH7.4 to the desired concentration, which was confirmed based on the A_{280} (ε_{280} = 91.9 $mM^{-1}cm^{-1}$).

The general experimental procedure was as follows: Fe(Mn)SOD solution was prepared in 50 mM potassium phosphate pH7.4 buffer to a final concentration of 9.98 μM and stored at 4°C. 1 ml enzyme solution was added to a cuvette (1cm path length), following by adding 20μL ABTS and 40μL EDTA stocks. The reaction was initiated by addition of H_2O_2 and the A_{415} was monitored continuously using a Cary 60 spectrophotometer in Kinetics mode.

5.2.2 Results and Discussions

The control experiments shown in Figure 5-2b indicated that the presence of enzyme, H_2O_2 and ABTS are necessary for the ABTS chromogenic assay. The growing absorption at 415nm reflected the generation of green-colored $ABTS^{\bullet+}$. The UV-Vis spectra of $ABTS^{\bullet+}$ were shown in the inset plot of Figure 5-2a. The data in Figure 5-1a show that the rate of formation of $ABTS^{\bullet+}$ increased with increasing H_2O_2 concentration. However it is seen that there was a lag period between initiation of the reaction and product formation, likely reflecting accumulation of a reaction intermediate[110]. The "back reaction" of $ABTS^{\bullet+}$ to regenerate ABTS also contributed to the later part of the time course produced by 30 mM H_2O_2 at ~10min. For the lower peroxide concentrations, a longer time might be needed to observe this back reaction. Given the slow reaction and the presence of a back reaction, accurate determination of the stoichiometry between H_2O_2 and ABTS has been difficult[110]. Kadnikova[116] proposed the equation below to describe the decay of $ABTS^{\bullet+}$ even though this reaction was far from clearly studied.

$$ABTS^{\bullet+} + \frac{1}{2}H_2O \rightarrow ABTS + \frac{1}{4}O_2 + H^+$$

However, H_2O_2 -treated FeSOD had completely different ABTS activity as shown in Figure 4.2b and $ABTS^{\bullet+}$ decay was observed at only select high peroxide concentrations. At high H_2O_2 concentration, the initial rate of $ABTS^{\bullet+}$ formation was higher but the maximal amount was lower, due to an accelerated radical decay rate. In Yamakura's paper, FeSOD was used as a negative control proving that FeSOD lacks ABTS activity. Our data suggested that FeSOD still exerts some ABTS activity, which is just too fast to monitor by normal UV-Vis absorption.

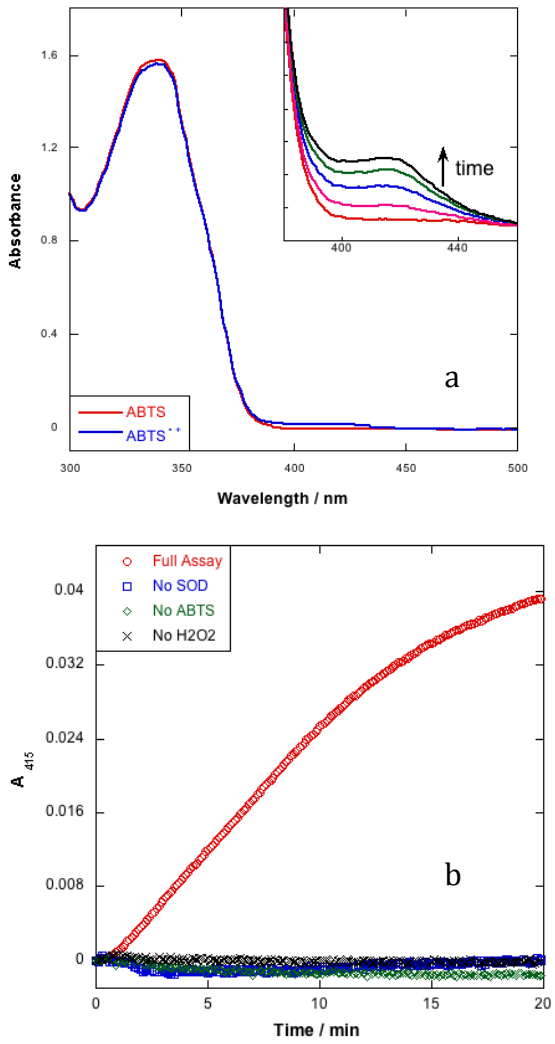

Figure 5-2 UV-Vis spectra of ABTS and ABTS$^{\bullet+}$.
(a) UV-Vis spectra of ABTS and ABTS$^{\bullet+}$ after H_2O_2 treatment. The inset plot displays the change of ABTS$^{\bullet+}$ spectra as a function of increasing time. (b) Control experiments for the ABTS assay. The time-dependent change of absorbance at 415nm is shown.

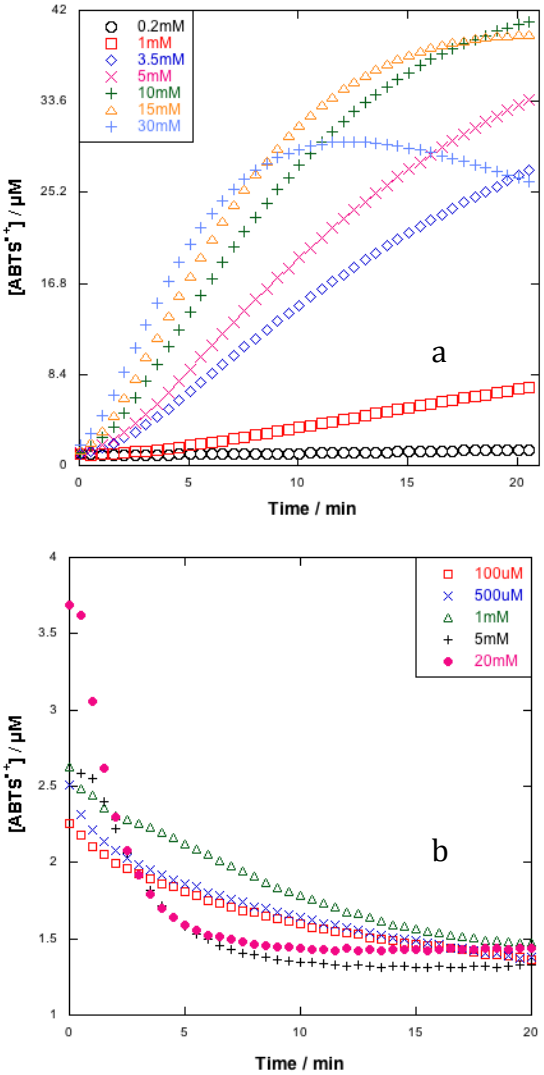

Figure 5-3 The time-dependence change of the $ABTS^{\bullet+}$.
The time-dependence of the $ABTS^{\bullet+}$ concentration in the presence of Fe(Mn)SOD (a) and FeSOD (b) and various concentrations of H_2O_2.

5.3 Amplex Red assay

To test for the possibility that our results were specific to ABTS, we also tested for peroxidase activity using a different commonly-used chromophoric peroxidase substrate: Amplex red. Amplex red is converted from a colorless/non-fluorescing compound to an intensely colored fluorescing complex, resorufin, by the action of peroxidases such as horseradish peroxidase (HRP) in the presence of H_2O_2. The resorufin concentration is measured at 571 nm (ε_{571} = 55 $mM^{-1}cm^{-1}$) [117]. As in the case of $ABTS^{+\bullet}$, resorufin is also a

substrate for peroxidases and is converted to a colorless/nonfluorescing molecule. The accepted mechanism of amplex red oxidation by HRP involves initial oxidization of Fe^{3+} by H_2O_2 to compound I, which is a highly reactive oxo-ferryl ($Fe^{IV} = O$) moiety in conjunction with a porphyrin radical. Compound I then oxidizes two equivalents of substrates such as ABTS or Amplex red as it reverts to the ferric form via another intermediate, compound II, in two one-electron steps.

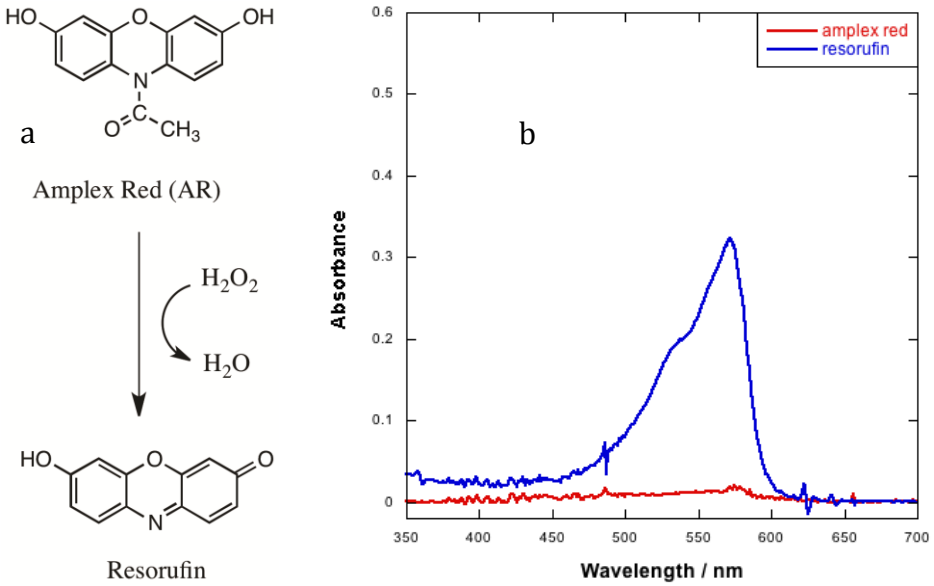

Figure 5-4 The structure and UV-Vis spectra of Amplex Red and Resorufin.

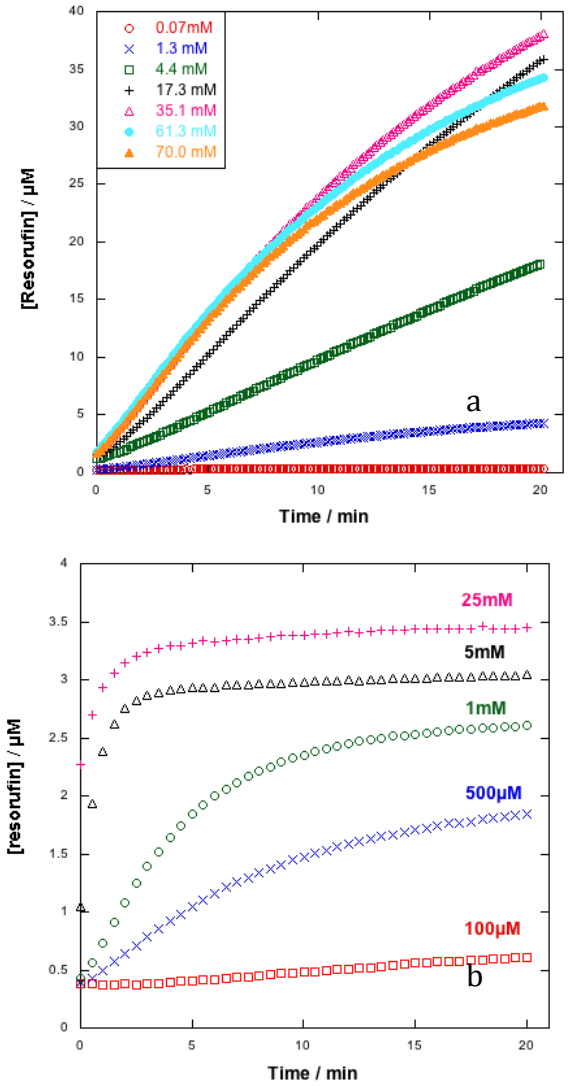

Figure 5-5 The time-dependence of Resorufin production.
The time-dependence of Resorufin concentration produced by the reaction of H_2O_2 with Fe(Mn)SOD (a) and FeSOD (b).

The spectrum of resorufin is shown in Figure 5-4b and displays a distinct peak at 572 nm. As the H_2O_2 concentration increases, the formation rate and yield of resorufin grew up to a maximum produced by 35.1 mM H_2O_2 as illustrated in Figure 5-5a. After that, the yields of resorufin were lessened, probably because of the consumption resorufin, which also serves as a peroxidase substrate when [H_2O_2] > [amplex red] [117]. The amplex red oxidizing activity of FeSOD is shown in Figure 5-5b and was unexpectedly low compared to that of Fe(Mn)SOD. At high H_2O_2 concentrations, the initial rate increased as

we expected, along with the maximal yield, however the maximal yield was much lower than in Fe(Mn)SOD. It was found that resorufin formation occurred within the dead time of the absorption measurement illustrated by the initial resorufin concentration at t=0. A similar observation was made with ABTS, indicating that the initial reaction with FeSOD in the presence of H_2O_2 is much faster than in the case of Fe(Mn)SOD, as illustrated by Figure 5-6. Related to the UV-Vis and EPR data in Chapter 3, we proposed that this fast reaction includes Fe^{3+} reduction by H_2O_2, which could then generate some highly reactive species that can oxidize ABTS and Amplex Red. However, we still cannot explain the difference between ABTS and Amplex Red activities.

Recent reports of Amplex Red autooxidation upon exposure to light in the absence of H_2O_2 and HPR raise concerns about the interpretation of our data [118,119] since the time dependences were monitored with cuvettes in a spectrophotometer. Trace amount of resorufin present in Amplex Red stock solution would initiate the self-oxidation reaction. The addition of active Cu,Zn-SOD that catalyzes the conversion of superoxide radical to H_2O_2 and O_2 dramatically increased the oxidation of Amplex Red [118,119]. Therefore the authors proposed that illumination of amplex red resulted in formation of superoxide and that the increased formation of H_2O_2 from dismutation of $O_2^{\bullet-}$ by SOD accounted for the oxidation of amplex red[118].

MnSOD-meidated peroxidase activity was reported based on the Amplex Red assay[120-122]. Formation of resorufin escalated with increased H_2O_2 concentration due to some kind of oxidative modification of the enzyme[120-122]. However, these conclusions were challenged by Liochev and Fridovich[123], who suggested that the autooxidation of Amplex Red rather than MnSOD peroxidase activity contributed to their observations.

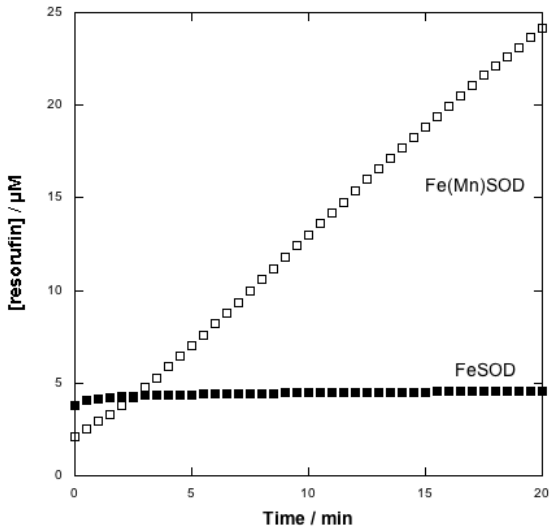

Figure 5-6 Comparison of resorufin production by Fe(Mn)SOD and FeSOD in the presence of H_2O_2.

5.4 O_2 production and H_2O_2 consumption

An abundance of bubbles was generated when Fe(Mn)SOD was exposed to H_2O_2. The most reasonable explanation was that oxygen gas was formed during the catalase reaction or the disproportion reaction of $O_2^{\bullet-}/HO_2^{\bullet-}$. To study the O_2 formation and H_2O_2 consumption, an oxygen electrode was used to monitor the change of O_2 and H_2O_2 concentrations in the solution.

Potassium phosphate buffer was degased in a glovebox by stirring overnight to remove most of the dissolved oxygen gas, to generate anaerobic buffer. Fe(Mn)SOD was diluted with anaerobic buffer and the concentration was determined by absorption at 280 nm. The H_2O_2 concentration was obtained by a 1000-fold dilution of the 30% stock solution and determination of the concentration via the absorption at 240 nm (ε_{240} = 34.6 $mM^{-1}cm^{-1}$). All the materials needed for the assay were moved into the glovebag, whose opening was then sealed. The glovebag was then exhausted by a vacuum pump to remove the air (shown in Figure 5-7) followed by refilling with Argon. Three cycles were performed and the glovebag was kept under Argon atmosphere for measurements. The change in the dissolved oxygen (DO) concentration in the anaerobic buffer was found to remain less than 10 µM after a day in the glove bag so prepared. The DO concentration of the Fe(Mn)SOD plus H_2O_2 solution

increased with time and depended on the H_2O_2 concentration as shown in Figure 5-9. For similar solutions lacking only Fe(Mn)SOD, there was almost no change in DO.

Figure 5-7 Photos of the experimental setup for dissolved O_2 measurements in the glovebag.

The concentrations of H_2O_2 were determined using ferrous thiocyanate method[124,125] based on the oxidization of ferrous ion to ferric ion, with some modification for our purposes. At low-pH, thiocyanate ion binds to ferric rion generating a red-colored complex that could be measured at 480 nm. Diluted Fe(Mn)SOD with different amounts of H_2O_2 was denatured by adding 10% trichloroacetic acid. After removal of precipitated protein by centrifugation at 12000 rpm for 2 min, 0.1 ml 2.5 M potassium thiocyanate was added to a 1.0 ml aliquot of the supernatant. Absorption at 480 nm was taken as the background absorbace A_0 resulting from Fe released by the protein. Because of the low

concentration of protein, A_0 was small and had little impact on the result. 0.2 ml 10 mM ferrous ammonium sulfate was added after measuring A_0, and incubated for ~20 min before A_1 at 480 nm was recorded. The chromogenic reaction reached equilibrium after incubation for 20 minutes generating a constant absorption. To calculate the H_2O_2 in the mixture, we constructed a standard curve using samples produced by the same protocol but containing known concentrations of H_2O_2 and no FeSOD or Fe(Mn)SDO, under the same condition as shown in Figure 5-8.

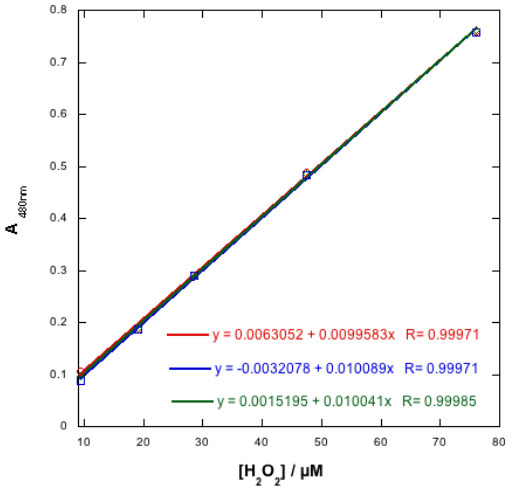

Figure 5-8 The standard curve of ferrous thiocyanate method from different trials.

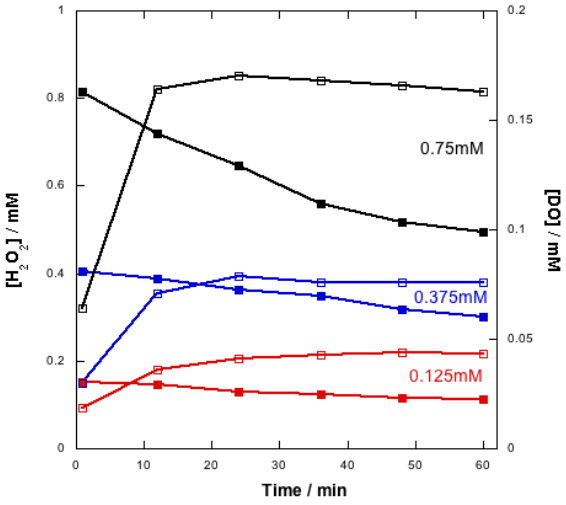

Figure 5-9 H_2O_2 consumption and O_2 formation.
H_2O_2 consumption and dissolved oxygen generation by Fe(Mn)SOD in the presence of different concentration of H_2O_2. The closed squares represent H_2O_2 concentrations and open squares represent dissolve O_2 concentrations.

The stoichiometric ratios of H_2O_2 consumed to O_2 produced were determined to be 2 H_2O_2 consumed per 1 O_2 formed over 60 min. This is consistent with catalase activity. However, the time dependencies indicated that the O_2 formation was most rapid during the first 10 min and then reached plateau or even decreased. The O_2 produced during the first 10 minutes compared to the H_2O_2 consumed during the same time interval yielded a different stoichiometry. H_2O_2 decreases over time were most rapid at high H_2O_2 concentrations. Therefore, within the first 10 min, much more O_2 was formed compared to the reacted H_2O_2 and we propose that the consumption of H_2O_2 corresponds to two different reactions in the course of the experiment. At short times we observe H_2O_2 -> O_2 but at later times H_2O_2 appears to be engaging in a different reaction. We note that when ABTS or amplex red were present there was no visible O_2 evolution, suggesting that the reaction with the chromogen outcompeted whatever reaction oxidizes H_2O_2 to O_2.

CONCLUSIONS

In this project, we used an *in vivo* preparation method to produce Fe(Mn)SOD that is inactive with respect to superoxide radical dismutation owing to the mis-incorporation of Fe in the active site evolved to use Mn. The properties of Fe(Mn)SOD were found to agree well with previous studies, even though less Fe incorporation was somewhat sub-stoichiometric. These results support the possibility of *in vivo* presence of Fe-substituted MnSOD in aerobic organisms or even in human mitochondria.

To investigate the possible toxicity of Fe(Mn)SOD via possible peroxidase activity, the reaction of Fe(Mn)SOD with hydrogen peroxide was studied, including the changes of optical spectra, modification of Trp residues, variations of active site coordination and secondary structures. I found that after exposure to H_2O_2, Trp residues were oxidized based on both UV-Vis signatures and near UV CD spectra. The secondary structure of the protein was also impacted, probably because of the modification of Trp residues. We could attribute these changes to reactions mediated by the active site Fe, because the results of H_2O_2 treatement were very different from those displayed by FeSOD. Although FeSOD's Trp also underwent modification and the enzyme became inactivated, the nature of the reactions with H_2O_2 was not identical. Even H_2O_2 is believed to oxidize proteins via highly reactive intermediates including Fe and formed via Fe^{2+} we were not able to observe Fe^{3+} reduction in Fe(Mn)SOD, although our methods succeeded in doing so in FeSOD. What's more, the activities of Fe(Mn)SOD and FeSOD were totally different in the ABTS assay or Amplex Red assay. Since several reactions contribute to absorbance changes observed in each of these assays, more work should be done to understand what reactions occur.

While additional studies employing shorter times and terminating the H_2O_2's reaction with the protein in advance of slower analyses are needed to capture the sequence of evens, it is already indisputable that the different active sites and reduction potentials of Fe(Mn)SOD and FeSOD play a decisive role in

determining the course of H_2O_2's reactions and the outcomes of treatment in those two homologous proteins.

REFERENCES

(1) Yamakura, F.; Kobayashi, K.; Furukawa, S.; Suzuki, Y. In vitro preparation of iron-substituted human manganese superoxide dismutase: Possible toxic properties for mitochondria. *Free Radical Bio Med* **2007**, *43*, 423-430.

(2) Touyz, R. M.; Schiffrin, E. L. Reactive oxygen species in vascular biology: implications in hypertension. *Histochem. Cell Biol.* **2004**, *122*, 339-352.

(3) Vanderkooi, J. M.; Erecinska, M.; Silver, I. A. OXYGEN IN MAMMALIAN TISSUE - METHODS OF MEASUREMENT AND AFFINITIES OF VARIOUS REACTIONS. *Am. J. Physiol.* **1991**, *260*, C1131-C1150.

(4) Brown, M. M.; Wade, J. P. H.; Marshall, J. FUNDAMENTAL IMPORTANCE OF ARTERIAL OXYGEN-CONTENT IN THE REGULATION OF CEREBRAL BLOOD-FLOW IN MAN. *Brain* **1985**, *108*, 81-93.

(5) Canfield, D. E.; Marais, D. J. D. BIOGEOCHEMICAL CYCLES OF CARBON, SULFUR, AND FREE OXYGEN IN A MICROBIAL MAT. *Geochim. Cosmochim. Acta* **1993**, *57*, 3971-3984.

(6) Apel, K.; Hirt, H. Reactive oxygen species: Metabolism, oxidative stress, and signal transduction. *Annu. Rev. Plant Biol.* **2004**, *55*, 373-399.

(7) Cadenas, E. BIOCHEMISTRY OF OXYGEN-TOXICITY. *Annu. Rev. Biochem.* **1989**, *58*, 79-110.

(8) Fridovich, I. BIOLOGICAL EFFECTS OF THE SUPEROXIDE RADICAL. *Arch Biochem Biophys* **1986**, *247*, 1-11.

(9) Turrens, J. F. Mitochondrial formation of reactive oxygen species. *J. Physiol.-London* **2003**, *552*, 335-344.

(10) Yu, B. P. CELLULAR DEFENSES AGAINST DAMAGE FROM REACTIVE OXYGEN SPECIES. *Physiol. Rev.* **1994**, *74*, 139-162.

(11) Chevion, M. A Site-Specific Mechanism for Free-Radical Induced Biological Damage - the Essential Role of Redox-Active Transition-Metals. *Free Radical Bio Med* **1988**, *5*, 27-37.

(12) Fridovic.I. QUANTITATIVE ASPECTS OF PRODUCTION OF SUPEROXIDE ANION RADICAL BY MILK XANTHINE OXIDASE. *J Biol Chem* **1970**, *245*, 4053-&.

(13) Hawkins, C. L.; Davies, M. J. Generation and propagation of radical reactions on proteins. *Bba-Bioenergetics* **2001**, *1504*, 196-219.

(14) Mcadam, M. E.; Fox, R. A.; Lavelle, F.; Fielden, E. M. Pulse-Radiolysis Study of Manganese-Containing Superoxide-Dismutase from Bacillus-Stearothermophilus - Kinetic-Model for Enzyme Action. *Biochem. J.* **1977**, *165*, 71-79.

(15) Takeda, Y.; Avila, H. Structure and Gene-Expression of the Escherichia-Coli Mn-Superoxide Dismutase Gene. *Nucleic Acids Res* **1986**, *14*, 4577-4589.

(16) Bowler, C.; Vanmontagu, M.; Inze, D. SUPEROXIDE-DISMUTASE AND STRESS TOLERANCE. *Annu. Rev. Plant Physiol. Plant Molec. Biol.* **1992**, *43*, 83-116.

(17) McCord, J. M.; Fridovic.I. SUPEROXIDE DISMUTASE AN ENZYMIC FUNCTION FOR ERYTHROCUPREIN (HEMOCUPREIN). *J Biol Chem* **1969**, *244*, 6049-&.

(18) Misra, H. P.; Fridovic.I. ROLE OF SUPEROXIDE ANION IN AUTOXIDATION OF EPINEPHRINE AND A SIMPLE ASSAY FOR SUPEROXIDE DISMUTASE. *J Biol Chem* **1972**, *247*, 3170-&.

(19) Marklund, S.; Marklund, G. INVOLVEMENT OF SUPEROXIDE ANION RADICAL IN AUTOXIDATION OF PYROGALLOL AND A CONVENIENT ASSAY FOR SUPEROXIDE-DISMUTASE. *Eur J Biochem* **1974**, *47*, 469-474.

(20) Fink, R. C.; Scandalios, J. G. Molecular evolution and structure-function relationships of the superoxide dismutase gene families in angiosperms and their relationship to other eukaryotic and prokaryotic superoxide dismutases. *Arch Biochem Biophys* **2002**, *399*, 19-36.

(21) Balzan, R.; Bannister, W. H.; Hunter, G. J.; Bannister, J. V. Escherichia-Coli Iron Superoxide-Dismutase Targeted to the Mitochondria of Yeast-Cells Protects the Cells against Oxidative Stress. *P Natl Acad Sci USA* **1995**, *92*, 4219-4223.

(22) Edward, R. A.; Whittaker, M. M.; Whittaker, J. W.; Jameson, G. B.; Baker, E. N. Distinct metal environment in Fe-substituted manganese superoxide dismutase provides a structural basis of metal specificity. *J Am Chem Soc* **1998**, *120*, 9684-9685.

(23) Vance, C. K.; Miller, A. F. Spectroscopic comparisons of the pH dependencies of Fe-substituted (Mn)superoxide dismutase and Fe-superoxide dismutase. *Biochemistry-Us* **1998**, *37*, 5518-5527.

(24) Vance, C. K.; Miller, A. F. Simple proposal that can explain the inactivity of metal-substituted superoxide dismutases. *J Am Chem Soc* **1998**, *120*, 461-467.

(25) Fee, J. A.; Mcclune, G. J.; Lees, A. C.; Zidovetzki, R.; Pecht, I. The Ph-Dependence of the Spectral and Anion Binding-Properties of Iron Containing Superoxide-Dismutase from Escherichia-Coli-B - an Explanation for the Azide Inhibition of Dismutase Activity. *Israel J Chem* **1981**, *21*, 54-58.

(26) Vanloon, A. P. G. M.; Pesoldhurt, B.; Schatz, G. A Yeast Mutant Lacking Mitochondrial Manganese-Superoxide Dismutase Is Hypersensitive to Oxygen. *P Natl Acad Sci USA* **1986**, *83*, 3820-3824.

(27) Lebovitz, R. M.; Zhang, H. J.; Vogel, H.; Cartwright, J.; Dionne, L.; Lu, N. F.; Huang, S.; Matzuk, M. M. Neurodegeneration, myocardial injury, and perinatal death in mitochondrial superoxide dismutase-deficient mice. *P Natl Acad Sci USA* **1996**, *93*, 9782-9787.

(28) Dhar, S. K.; St. Clair, D. K. Manganese superoxide dismutase regulation and cancer. *Free Radical Bio Med*, *52*, 2209-2222.

(29) Yang, M.; Cobine, P. A.; Molik, S.; Naranuntarat, A.; Lill, R.; Winge, D. R.; Culotta, V. C. The effects of mitochondrial iron homeostasis on cofactor specificity of superoxide dismutase 2. *Embo J* **2006**, *25*, 1775-1783.

(30) Luk, E.; Carroll, M.; Baker, M.; Culotta, V. C. Manganese activation of superoxide dismutase 2 in Saccharomyces cerevisiae requires MTM1, a member of the mitochondrial carrier family. *P Natl Acad Sci USA* **2003**, *100*, 10353-10357.

(31) Pierrel, F.; Cobine, P. A.; Winge, D. R. Metal Ion availability in mitochondria. *Biometals* **2007**, *20*, 675-682.

(32) Beyer, W. F.; Fridovich, I. Invivo Competition between Iron and Manganese for Occupancy of the Active-Site Region of the Manganese-Superoxide Dismutase of Escherichia-Coli. *J Biol Chem* **1991**, *266*, 303-308.

(33) Clare, D. A.; Blum, J.; Fridovich, I. A Hybrid Superoxide-Dismutase Containing Both Functional Iron and Manganese. *J Biol Chem* **1984**, *259*, 5932-5936.

(34) Privalle, C. T.; Fridovich, I. Transcriptional and Maturational Effects of Manganese and Iron on the Biosynthesis of Manganese-Superoxide Dismutase in Escherichia-Coli. *J Biol Chem* **1992**, *267*, 9140-9145.

(35) Takao, M.; Yasui, A.; Oikawa, A. Unique Characteristics of Superoxide-Dismutase of a Strictly Anaerobic Archaebacterium Methanobacterium-Thermoautotrophicum. *J Biol Chem* **1991**, *266*, 14151-14154.

(36) Whittaker, M. M.; Whittaker, J. W. Mutagenesis of a proton linkage pathway in Escherichia coli manganese superoxide dismutase. *Biochemistry-Us* **1997**, *36*, 8923-8931.

(37) Whittaker, J. W. Metal uptake by manganese superoxide dismutase. *Bba-Proteins Proteom* **2010**, *1804*, 298-307.

(38) Whittaker, M. M.; Lerch, T. F.; Kirillova, O.; Chapman, M. S.; Whittaker, J. W. Subunit dissociation and metal binding by Escherichia coil apo-manganese superoxide dismutase. *Arch Biochem Biophys* **2011**, *505*, 213-225.

(39) Whittaker, M. M.; Whittaker, J. W. Conformationally Gated Metal Uptake by Apomanganese Superoxide Dismutase. *Biochemistry-Us* **2008**, *47*, 11625-11636.

(40) Whittaker, M. M.; Whittaker, J. W. In vitro metal uptake by recombinant human manganese superoxide dismutase. *Arch Biochem Biophys* **2009**, *491*, 69-74.

(41) Whittaker, M. M.; Whittaker, J. W. Metallation state of human manganese superoxide dismutase expressed in Saccharomyces cerevisiae. *Arch Biochem Biophys* **2012**, *523*, 191-197.

(42) Whittaker, J. W. The irony of manganese superoxide dismutase. *Biochem Soc T* **2003**, *31*, 1318-1321.

(43) Dooley, D. M.; Karas, J. L.; Jones, T. F.; Cote, C. E.; Smith, S. B. Reactions of H2o2 with the Iron-Containing Superoxide-Dismutase from Escherichia-Coli. *Inorg Chem* **1986**, *25*, 4761-4766.

(44) Yamakura, F.; Suzuki, K. Inactivation of Pseudomonas Iron-Superoxide Dismutase by Hydrogen-Peroxide. *Biochim Biophys Acta* **1986**, *874*, 23-29.

(45) Beyer, W. F.; Fridovich, I. Effect of Hydrogen-Peroxide on the Iron-Containing Superoxide-Dismutase of Escherichia-Coli. *Biochemistry-Us* **1987**, *26*, 1251-1257.

(46) Rao, P. S.; Simic, M.; Hayon, E. Pulse-Radiolysis Study of Imidazole and Histidine in Water. *J Phys Chem-Us* **1975**, *79*, 1260-1263.

(47) Bannister, J. V.; Bannister, W. H.; Rotilio, G. Aspects of the Structure, Function, and Applications of Superoxide-Dismutase. *Crit Rev Biochem Mol* **1987**, *22*, 111-180.

(48) Lah, M. S.; Dixon, M. M.; Pattridge, K. A.; Stallings, W. C.; Fee, J. A.; Ludwig, M. L. Structure-Function in Escherichia-Coli Iron Superoxide-Dismutase - Comparisons with the Manganese Enzyme from Thermus-Thermophilus. *Biochemistry* **1995**, *34*, 1646-1660.

(49) Grove, L. E.; Xie, J.; Yikilmaz, E.; Karapetyan, A.; Miller, A. F.; Brunold, T. C. Spectroscopic and computational insights into second-sphere amino-acid tuning of substrate analogue/active-site interactions in iron(III) superoxide dismutase. *Inorg Chem* **2008**, *47*, 3993-4004.

(50) Jackson, T. A.; Gutman, C. T.; Maliekal, J.; Miller, A. F.; Brunold, T. C. Geometric and Electronic Structures of Manganese-Substituted Iron Superoxide Dismutase. *Inorg Chem* **2013**, *52*, 3356-3367.

(51) Benov, L.; Fridovich, I. Growth in iron-enriched medium partially compensates Escherichia coli for the lack of manganese and iron superoxide dismutase. *J Biol Chem* **1998**, *273*, 10313-10316.

(52) Slykhouse, T. O.; Fee, J. A. Physical and Chemical Studies on Bacterial Superoxide Dismutases - Purification and Some Anion Binding Properties of Iron-Containing Protein of Escherichia-Coli-B. *J Biol Chem* **1976**, *251*, 5472-5477.

(53) Davis, B. J. Disc Electrophoresis .2. Method and Application to Human Serum Proteins. *Ann Ny Acad Sci* **1964**, *121*, 404-&.

(54) Glasel, J. A. Validity of nucleic acid purities monitored by 260/280 absorbance ratios. *Biotechniques* **1995**, *18*, 62-63.

(55) Wilfinger, W.; Mackey, K.; Chomczynski, P. Effect of pH and salt concentration on the A(260/280) ratio of nucleic acids. *Mol. Biol. Cell* **1996**, *7*, 926-926.

(56) Beaucham.C; Fridovic.I. Superoxide Dismutase - Improved Assays and an Assay Applicable to Acrylamide Gels. *Anal. Biochem.* **1971**, *44*, 276-&.

(57) Yocum, C. F.; Yerkes, C. T.; Blankenship, R. E.; Sharp, R. R.; Babcock, G. T. Stoichiometry, Inhibitor Sensitivity, and Organization of Manganese Associated with Photosynthetic Oxygen Evolution. *P Natl Acad Sci-Biol* **1981**, *78*, 7507-7511.

(58) Towbin, H.; Staehelin, T.; Gordon, J. ELECTROPHORETIC TRANSFER OF PROTEINS FROM POLYACRYLAMIDE GELS TO NITROCELLULOSE SHEETS - PROCEDURE AND SOME APPLICATIONS. *P Natl Acad Sci USA* **1979**, *76*, 4350-4354.

(59) Weber, K.; Osborn, M. RELIABILITY OF MOLECULAR WEIGHT DETERMINATIONS BY DODECYL SULFATE-POLYACRYLAMIDE GEL ELECTROPHORESIS. *J Biol Chem* **1969**, *244*, 4406-&.

(60) Beaucham.C; Fridovic.I. New Assay for Superoxide Dismutase, Applicable to Polyacrylamide Gels. *Fed Proc* **1971**, *30*, 1233-&.

(61) Kuo, C. F.; Fridovich, I. A Stain for Iron-Containing Proteins Sensitive to Nanogram Levels of Iron. *Anal. Biochem.* **1988**, *170*, 183-185.

(62) Carter, P. Spectrophotometric Determination of Serum Iron at Submicrogram Level with a New Reagent (Ferrozine). *Anal. Biochem.* **1971**, *40*, 450-&.

(63) Yamakura, F.; Kobayashi, K.; Ue, H.; Konno, M. The Ph-Dependent Changes of the Enzymatic-Activity and Spectroscopic Properties of Iron-Substituted Manganese Superoxide-Dismutase - a Study on the Metal-Specific Activity of Mn-Containing Superoxide-Dismutase. *Eur J Biochem* **1995**, *227*, 700-706.

(64) Palmer, G. The Electron-Paramagnetic Resonance of Metalloproteins. *Biochem Soc T* **1985**, *13*, 548-560.

(65) Yang, A. S.; Gaffney, B. J. Determination of Relative Spin Concentration in Some High-Spin Ferric Proteins Using E/D-Distribution in Electron-Paramagnetic Resonance Simulations. *Biophys. J.* **1987**, *51*, 55-67.

(66) Neese, F.; Solomon, E. I. Detailed spectroscopic and theoretical studies on [Fe(EDTA)(O(2))](3-): Electronic structure of the side-on ferric-peroxide bond and its relevance to reactivity. *J Am Chem Soc* **1998**, *120*, 12829-12848.

(67) Ose, D. E.; Fridovich, I. Manganese-Containing Superoxide-Dismutase from Escherichia-Coli - Reversible Resolution and Metal Replacements. *Arch Biochem Biophys* **1979**, *194*, 360-364.

(68) Whittaker, M. M.; Whittaker, J. W. Low-temperature thermochromism marks a change in coordination for the metal ion in manganese superoxide dismutase. *Biochemistry-Us* **1996**, *35*, 6762-6770.

(69) Oberley, L. W.; Buettner, G. R. Role of Superoxide-Dismutase in Cancer - Review. *Cancer Res* **1979**, *39*, 1141-1149.

(70) Dhar, S. K.; Tangpong, J.; Chaiswing, L.; Oberley, T. D.; St Clair, D. K. Manganese Superoxide Dismutase Is a p53-Regulated Gene That Switches Cancers between Early and Advanced Stages. *Cancer Res* **2011**, *71*, 6684-6695.

(71) Sun, Y.; Holley, A. K.; St. Clair, D. K. p53 Regulation of Energy Metabolism and Mitochondria Regulation of p53 in Cancer Cells: An Insight into the Role of Manganese Superoxide Dismutase. *Current Pharmaceutical Biotechnology* **2013**, *14*, 261-273.

(72) Wetlaufer, D. B. Ultraviolet Spectra of Proteins and Amino Acids. *Adv Protein Chem* **1962**, *17*, 303-390.

(73) Knox, W. E. TRYPTOPHAN OXIDATION. *Methods Enzymol.* **1955**, *2*, 242-253.

(74) Zhang, H.; Andrekopoulos, C.; Joseph, J.; Chandran, K.; Karoui, H.; Crow, J. P.; Kalyanaraman, B. Bicarbonate-dependent peroxidase activity of human Cu, Zn-superoxide dismutase induces covalent aggregation of protein - Intermediacy of tryptophan-derived oxidation products. *J Biol Chem* **2003**, *278*, 24078-24089.

(75) Bull, C.; Mcclune, G. J.; Fee, J. A. The Mechanism of Fe-Edta Catalyzed Superoxide Dismutation. *J Am Chem Soc* **1983**, *105*, 5290-5300.

(76) Chen, Y. H.; Yang, J. T. New Approach to Calculation of Secondary Structures of Globular Proteins by Optical Rotatory Dispersion and Circular Dichroism. *Biochem Bioph Res Co* **1971**, *44*, 1285-&.

(77) Greenfield, N. J. Applications of circular dichroism in protein and peptide analysis. *Trac-Trend Anal Chem* **1999**, *18*, 236-244.

(78) Chang, C. T.; Wu, C. S. C.; Yang, J. T. Circular Dichroic Analysis of Protein Conformation - Inclusion of Beta-Turns. *Anal. Biochem.* **1978**, *91*, 13-31.

(79) Chakrabartty, A.; Kortemme, T.; Padmanabhan, S.; Baldwin, R. L. AROMATIC SIDE-CHAIN CONTRIBUTION TO FAR-ULTRAVIOLET CIRCULAR-DICHROISM OF HELICAL PEPTIDES AND ITS EFFECT ON MEASUREMENT OF HELIX PROPENSITIES. *Biochemistry-Us* **1993**, *32*, 5560-5565.

(80) de Planque, M. R. R.; Kruijtzer, J. A. W.; Liskamp, R. M. J.; Marsh, D.; Greathouse, D. V.; Koeppe, R. E.; de Kruijff, B.; Killian, J. A. Different membrane anchoring positions of tryptophan and lysine in synthetic transmembrane alpha-helical peptides. *J Biol Chem* **1999**, *274*, 20839-20846.

(81) Kahn, P. C.: [16] The interpretation of near-ultraviolet circular dichroism. In *Methods Enzymol.*; C.H.W. Hirs, S. N. T., Ed.; Academic Press, 1979; Vol. Volume 61; pp 339-378.

(82) Kay, E.; Strickla.Eh; Billups, C. Near Ultraviolet Circular-Dichroism and Absorption-Spectra of Chicken Ovomucoid and Acetylated Derivatives at 297 and 77 Degrees K. *J Biol Chem* **1974**, *249*, 797-802.

(83) Li, R.; Nagai, Y.; Nagai, M. Changes of tyrosine and tryptophan residues in human hemoglobin by oxygen binding: near- and far-UV circular dichroism of isolated chains and recombined hemoglobin. *J Inorg Biochem* **2000**, *82*, 93-101.

(84) Burstein, E. A.; Vedenkin.Ns; Ivkova, M. N. FLUORESCENCE AND LOCATION OF TRYPTOPHAN RESIDUES IN PROTEIN MOLECULES. *Photochemistry and Photobiology* **1973**, *18*, 263-279.

(85) Chen, Y.; Barkley, M. D. Toward understanding tryptophan fluorescence in proteins. *Biochemistry-Us* **1998**, *37*, 9976-9982.

(86) Meier, B.; Sehn, A. P.; Michel, C.; Saran, M. Reactions of Hydrogen-Peroxide with Superoxide-Dismutase from Propionibacterium-Shermanii - an Enzyme Which Is Equally Active with Iron or Manganese - Are Independent of the Prosthetic Metal. *Arch Biochem Biophys* **1994**, *313*, 296-303.

(87) Yamakura, F. Study on Reconstitution of Iron Superoxide Dismutase from Pseudomonas-Ovalis. *Journal of Biochemistry* **1978**, *83*, 849-857.

(88) James, N. G.; Byme, S. L.; Steere, A. N.; Smith, V. C.; MacGillivray, R. T. A.; Mason, A. B. Inequivalent Contribution of the Five Tryptophan Residues in the C-Lobe of Human Serum Transferrin to the Fluorescence Increase when Iron is Released. *Biochemistry-Us* **2009**, *48*, 2858-2867.

(89) Wang, F.; Lothrop, A. P.; James, N. G.; Griffiths, T. A. M.; Lambert, L. A.; Leverence, R.; Kaltashov, I. A.; Andrews, N. C.; MacGillivray, R. T. A.; Mason, A. B. A novel murine protein with no effect on iron homoeostasis is homologous with transferrin and is the putative inhibitor of carbonic anhydrase. *Biochem. J.* **2007**, *406*, 85-95.

(90) Whittaker, M. M.; Mizuno, K.; Bachinger, H. P.; Whittaker, J. W. Kinetic analysis of the metal binding mechanism of Escherichia coli manganese superoxide dismutase. *Biophys. J.* **2006**, *90*, 598-607.

(91) Lavelle, F.; McAdam, M. E.; Fielden, E. M.; Roberts, P. B.; Puget, K.; Michelson, A. M. PULSE-RADIOLYSIS STUDY OF CATALYTIC MECHANISM OF IRON-CONTAINING SUPEROXIDE-DISMUTASE FROM PHOTOBACTERIUM-LEIOGNATHI. *Biochem. J.* **1977**, *161*, 3-11.

(92) Morimoto, A.; Tanaka, M.; Takahashi, S.; Ishimori, K.; Hori, H.; Morishima, I. Detection of a tryptophan radical as an intermediate species in the reaction of horseradish peroxidase mutant (Phe-221 -> Trp) and hydrogen peroxide. *J Biol Chem* **1998**, *273*, 14753-14760.

(93) Hori, H.; Yonetani, T. Powder and Single-Crystal Electron-Paramagnetic Resonance Studies of Yeast Cytochrome-C Peroxidase and Its Peroxide Compound, Compound Es. *J Biol Chem* **1985**, *260*, 349-355.

(94) Yamakura, F. Destruction of Tryptophan Residues by Hydrogen-Peroxide in Iron-Superoxide Dismutase. *Biochem Bioph Res Co* **1984**, *122*, 635-641.

(95) Yamakura, F.; Rardin, R. L.; Petsko, G. A.; Ringe, D.; Hiraoka, B. Y.; Nakayama, K.; Fujimura, T.; Taka, H.; Murayama, K. Inactivation and destruction of conserved Trp159 of Fe-superoxide dismutase from Porphyromonas gingivalis by hydrogen peroxide. *Eur J Biochem* **1998**, *253*, 49-56.

(96) Goldstone, A. B.; Liochev, S. I.; Fridovich, I. Inactivation of Copper, Zinc superoxide dismutase by H2O2: Mechanism of protection. *Free Radical Bio Med* **2006**, *41*, 1860-1863.

(97) Liochev, S. I.; Fridovich, I. Mechanism of the peroxidase activity of Cu, Zn superoxide dismutase. *Free Radical Bio Med* **2010**, *48*, 1565-1569.

(98) Liochev, S. I.; Fridovich, I. A story of Cu,Zn superoxide dismutase, peroxymonocarbonate, and pseudo-second-order rate constants. *Free Radical Bio Med* **2012**, *53*, 1988-1990.

(99) Ramirez, D. C.; Mejiba, S. E. G.; Mason, R. P. Mechanism of hydrogen peroxide-induced Cu,Zn-superoxide dismutase-centered radical formation as explored by immuno-spin trapping: the role of copper- and carbonate radical anion-mediated oxidations. *Free Radical Bio Med* **2005**, *38*, 201-214.

(100) Yim, M. B.; Chock, P. B.; Stadtman, E. R. Enzyme Function of Copper, Zinc Superoxide-Dismutase as a Free-Radical Generator. *J Biol Chem* **1993**, *268*, 4099-4105.

(101) Prousek, J. Fenton chemistry in biology and medicine. *Pure Appl Chem* **2007**, *79*, 2325-2338.

(102) Kurtz, D. M. Avoiding high-valent iron intermediates: Superoxide reductase and rubrerythrin. *J Inorg Biochem* **2006**, *100*, 679-693.

(103) Gabbianelli, R.; Battistoni, A.; Capo, C.; Polticelli, F.; Rotilio, G.; Meier, B.; Desideri, A. Effect of Val73->Trp mutation on the reaction of "cambialistic" superoxide dismutase from Propionibacterium shermanii with hydrogen peroxide. *Arch Biochem Biophys* **1997**, *345*, 156-159.

(104) Beyer, W. F.; Fridovich, I.; Mullenbach, G. T.; Hallewell, R. Examination of the Role of Arginine-143 in the Human Copper and Zinc Superoxide-Dismutase by Site-Specific Mutagenesis. *J Biol Chem* **1987**, *262*, 11182-11187.

(105) Gross, A. J.; Sizer, I. W. Oxidation of Tyramine, Tyrosine, and Related Compounds by Peroxidase. *J Biol Chem* **1959**, *234*, 1611-1614.

(106) Gunther, M. R.; Peters, J. A.; Sivaneri, M. K. Histidinyl radical formation in the self-peroxidation reaction of bovine copper-zinc superoxide dismutase. *J Biol Chem* **2002**, *277*, 9160-9166.

(107) Liochev, S. I.; Fridovich, I. Copper, zinc superoxide dismutase and H2O2 - Effects of bicarbonate on inactivation and oxidations of NADPH and urate, and on consumption of H2O2. *J Biol Chem* **2002**, *277*, 34674-34678.

(108) Childs, R. E.; Bardsley, W. G. Steady-State Kinetics of Peroxidase with 2,2'-Azino-Di-(3-Ethylbenzthiazoline-6-Sulphonic Acid) as Chromogen. *Biochem. J.* **1975**, *145*, 93-103.

(109) Gallati, H. HORSERADISH-PEROXIDASE - STUDY OF THE KINETICS AND THE DETERMINATION OF OPTIMAL REACTION CONDITIONS, USING HYDROGEN-PEROXIDE AND 2,2-AZINO-BIS 3-ETHYLBENZTHIAZOLINE-6-SULFONIC ACID (ABTS) AS SUBSTRATES. *J Clin Chem Clin Bio* **1979**, *17*, 1-7.

(110) Rodriguez-Lopez, J. N.; Lowe, D. J.; Hernandez-Ruiz, J.; Hiner, A. N. P.; Garcia-Canovas, F.; Thorneley, R. N. F. Mechanism of reaction of hydrogen peroxide with horseradish peroxidase: Identification of intermediates in the catalytic cycle. *J Am Chem Soc* **2001**, *123*, 11838-11847.

(111) Lee, C.; Yoon, J. UV direct photolysis of 2,2 '-azino-bis(3-ethylbenzothiazoline-6-sulfonate) (ABTS) in aqueous solution: Kinetics and mechanism. *J Photoch Photobio A* **2008**, *197*, 232-238.

(112) Re, R.; Pellegrini, N.; Proteggente, A.; Pannala, A.; Yang, M.; Rice-Evans, C. Antioxidant activity applying an improved ABTS radical cation decolorization assay. *Free Radical Bio Med* **1999**, *26*, 1231-1237.

(113) Daquino, M.; Dunster, C.; Willson, R. L. Vitamin-a and Glutathione-Mediated Free-Radical Damage - Competing Reactions with Poly-Unsaturated Fatty-Acids and Vitamin-C. *Biochem Bioph Res Co* **1989**, *161*, 1199-1203.

(114) Lee, Y.; Yoon, J.; Von Gunten, U. Spectrophotometric determination of ferrate (Fe(Vl)) in water by ABTS. *Water Res* **2005**, *39*, 1946-1953.

(115) Prongjit, M.; Sucharitakul, J.; Wongnate, T.; Haltrich, D.; Chaiyen, P. Kinetic Mechanism of Pyranose 2-Oxidase from Trametes multicolor. *Biochemistry-Us* **2009**, *48*, 4170-4180.

(116) Kadnikova, E. N.; Kostic, N. M. Oxidation of ABTS by hydrogen peroxide catalyzed by horseradish peroxidase encapsulated into sol-gel glass. Effects of glass matrix on reactivity. *J Mol Catal B-Enzym* **2002**, *18*, 39-48.

(117) Reszka, K. J.; Wagner, B. A.; Burns, C. P.; Britigan, B. E. Effects of peroxidase substrates on the Amplex red/peroxidase assay: Antioxidant properties of anthracyclines. *Anal. Biochem.* **2005**, *342*, 327-337.

(118) Zhao, B. Z.; Summers, F. A.; Mason, R. P. Photooxidation of Amplex red to resorufin: Implications of exposing the Amplex red assay to light. *Free Radical Bio Med* **2012**, *53*, 1080-1087.

(119) Summers, F. A.; Zhao, B. Z.; Ganini, D.; Mason, R. P. Photooxidation of Amplex Red to Resorufin: Implications of Exposing the Amplex Red Assay to Light. *Hydrogen Peroxide and Cell Signaling, Part A* **2013**, *526*, 1-17.

(120) Ansenberger-Fricano, K.; Ganini, D.; Mao, M.; Chatterjee, S.; Dallas, S.; Mason, R. P.; Stadler, K.; Santos, J. H.; Bonini, M. G. The peroxidase activity of mitochondrial superoxide dismutase. *Free Radical Bio Med* **2013**, *54*, 116-124.

(121) Bayir, H.; Amoscato, A.; Rafikov, R.; Glumac, A.; Belikova, N.; Kagan, V. E. A novel mechanism of manganese superoxide dismutase (MNSOD) structural adaptation to oxidative and nitrative stress. *Crit Care Med* **2007**, *35*, A31-A31.

(122) Bayir, H.; Kagan, V. E.; Clark, R. S. B.; Janesko-Feldman, K.; Rafikov, R.; Huang, Z. T.; Zhang, X. J.; Vagni, V.; Billiar, T. R.; Kochanek, P. M. Neuronal NOS-mediated nitration and inactivation of manganese superoxide dismutase in brain after experimental and human brain injury. *J Neurochem* **2007**, *101*, 168-181.

(123) Liochev, S. I.; Fridovich, I. Peroxidase activity by MnSOD? *Free Radical Bio Med* **2013**, *65*, 1535-1535.

(124) Mishin, V.; Gray, J. P.; Heck, D. E.; Laskin, D. L.; Laskin, J. D. Application of the Amplex red/horseradish peroxidase assay to measure hydrogen peroxide generation by recombinant microsomal enzymes. *Free Radical Bio Med* **2010**, *48*, 1485-1491.

(125) Thurman, R. G.; Scholz, R.; Ley, H. G. Hepatic Microsomal Ethanol Oxidation - Hydrogen-Peroxide Formation and Role of Catalase. *Eur J Biochem* **1972**, *25*, 420-&.

VITA

Author's Name: Jianing Wang

Education

M.S.	Chemistry, University of Kentucky, Lexington, KY, USA, 2011-present
M. S.	Physical Chemistry, Beijing University of Technology, China, 2008-2011
B. S.	Applied Chemistry, Qingdao Agriculture University, China, 2004-2008

Professional experience

2011-2014	Teaching Assistant, Department of Chemistry, University of Kentucky, Lexington, KY, USA
2009-2011	Research Fellow, Department of Chemistry and Chemical Engineering, Beijing University of Technology, Beijing, China

Professional publications

Article • Effect of the Morphology of Pt Nanoparticles of Supported Pt Model Catalysts on CO Oxidation. Chin. J. Catal. 2011, 32:1329-1335 (http://www.sciencedirect.com/science/journal/18722067)

• The Peroxidase Activity of Fe(Mn)SOD and Possible Toxicity for Mitochondria. In Preparation.

Poster • The Effect of Hydrogen Peroxide on the Iron-substituted Manganese Superoxide Dismutase. 246th American Chemical Society National Meeting & Exposition, Indianapolis 2013

• A Comparative Study of More Efficient Methods for Purification of Superoxide Dismutase Protein, 32th Midwest Enzyme Chemistry Conference. Chicago, 2012

- Preparation of Well-defined Cubic Platinum Catalyst and Carbon Monoxide Oxidation. The Sixth Tokyo Conference on Advanced Catalytic Science and Technology & The Fifth Asia Pacific Congress on Catalysis (TOCAT6-APCAT6), Sapporo 2010